Spring 2021

Structural Insights into Heterodimerization and Catalysis of the Human Cis- prenyltransferase “NgBR/DHDDS” Complex

Ban H. Edani
Yale University Graduate School of Arts and Sciences, abdulrazaqb1@gmail.com

Abstract

Structural Insights into Heterodimerization and Catalysis of the Human *Cis*-prenyltransferase "NgBR/DHDDS" Complex

Ban Edani

2021

Cis-prenyltransferses (*cis*-PTases) constitute a family of enzymes involved in the synthesis of isoprenoid lipids required for various biological functions across all domains of life. The eukaryotic *cis*-PTase catalyzes the rate-limiting step in the synthesis of dolichyl phosphate, an indispensable glycosyl carrier lipid required for protein glycosylation in the lumen of endoplasmic reticulum. Based on enzyme composition, *cis*-PTases can be either homomeric or heteromeric enzymes. The human *cis*-PTase possesses a heteromeric configuration consisting of the two evolutionary related subunits: NgBR (dehydrodolichyl diphosphate synthase accessory subunit, first identified as a Nogo-B receptor) and DHDDS (dehydrodolichyl diphosphate synthase catalytic subunit). Recently, several mutations in both subunits have been reported to associate with various human diseases, collectively known as congenital disorders of glycosylation (CDG), including severe CDG type I, developmental and epileptic encephalopathy, and autosomal recessive retinitis pigmentosa. In addition, mutations on the NgBR subunit have been recently reported in patients suffering from early onset of Parkinson's disease (EOPD).

Despite its crucial role in the protein glycosylation process, the molecular mechanism of heteromeric *cis*-PTases remains poorly understood due to lack of structural-functional studies on these enzymes, in contrast to homodimeric *cis*-PTases which have been extensively studied. Therefore, in this dissertation, I illustrate the first crystal structure of a heteromeric, human *cis*-

PTase NgBR/DHDDS complex solved at 2.3 Å. The structure revealed novel features that were not previously observed in homodimeric enzymes, including a new dimeric interface formed by a unique C-terminus in DHDDS and a novel N-terminal segment in DHDDS serving as a membrane sensor for lipid activation. In addition, the structure elucidated the molecular details associated with substrate binding, catalysis, and disease-causing mutations. Finally, the structure provided novel insights into the mechanism of product chain elongation, an interesting yet one of the most enigmatic topics on prenyl chain elongating enzymes. In summary, the crystal structure advances our understanding of the molecular mechanism of heteromeric *cis*-PTase enzymes.

Structural Insights into Heterodimerization and Catalysis of the Human *Cis*-prenyltransferase "NgBR/DHDDS" Complex

A Dissertation
Presented to the Faculty of the Graduate School
of
Yale University
In Candidacy for the Degree of
Doctor of Philosophy

By
Ban Edani

Dissertation Director: Dr. William C. Sessa

June 2021

TABLE OF CONTENTS

Abstract……i

Table of Contents……iii

Table of Figures and Tables……v

Acknowledgements……vii

Chapter 1: Introduction ……...1

1.1 Isoprenoid biosynthesis ……...1

1.2 *Cis*-prenyltransferase: enzymatic reaction and classification…….....2

1.3 Evidence for the heteromeric organization of eukaryotic *cis*-PTase …….....3

1.4 The molecular mechanism of heteromeric *cis*-PTase remains elusive ……...6

1.5 Genetic disorders associated with *cis*-PTase loss-of-function mutations ……...8

1.6 NgBR regulation and cancer prognosis ……..9

1.7 Thesis aims.……...11

Chapter 2: The Crystal Structure of Human *cis*-PTase (NgBR/DHDDS) Complex Reveals Novel Insights into the Molecular Mechanism of Heteromeric Enzymes…..……..13

2.1 Introduction …….....13

2.2 Materials and Methods ……..16

2.3 Results …….....22

2.3.1 The core catalytic domain of NgBR/DHDDS complex…….22

2.3.2 Overall structure of the heteromeric complex…….....25

2.3.3 The active site of NgBR/DHDDS complex…….....30

2.3.4 Mapping disease mutations associated with the active site of NgBR/DHDDS complex…….....34

2.3.5 NgBR mutations and Parkinson's disease…….....37

2.3.6 Regulation of *cis*-PTase activity by membrane binding…….....40

2.3.7 The mechanism of product chain elongation…….44

2.4 Discussion and Future Direction. …….49

SI Appendix ……..56

References …….....73

TABLE OF FIGURES AND TABLES

Figure 2.1 The catalytic core domain of human *cis*-PTase ……...24

Figure 2.2 The overall structure of NgBR/DHDDS heterodimer……..28

Figure 2.3 The active site of the NgBR/DHDDS complex……33

Figure 2.4 Missense NgBR mutations associated with Parkinson's disease…….39

Figure 2.5 DHDDS's helix α0 functions as a membrane sensor……...42

Figure 2.6 Mechanism of chain elongation by heteromeric *cis*-PTases……47

Figure S1. De novo synthesis of dolichol from FPP and IPP……...56

Figure S2. Structural details of the NgBR subunit……57

Figure S3. Structural details of the DHDDS subunit ……58

Figure S4. Structural comparison of NgBR, Nus1and UPPS……59

Figure S5. Active site comparison of NgBR, DHDDS and UPPS……60

Figure S6. The final $2F_o$-F_c map surrounding the bound ligands……..61

Figure S7. Comparison of different dimeric structures……62

Figure S8. Limited proteolysis of NgBR/DHDDS complex …….....63

Figure S9. The dimeric interphase between NgBR and DHDDS …….64

Figure S10. The complete binding interactions for IPP1 and IPP2 ……..65

Figure S11. Structural comparison of the S1 site ……66

Figure S12. Structural comparison of the S2 site …….67

Figure S13. Missense mutations associated with CDG…….68

Figure S14. De novo DHDDS missense mutations associated with neurodegenerative disorder …….69

Figure S15. Plausible catalytic mechanism of the human NgBR/DHDDS complex……71

Table S1. Crystallographic Statistics ……**.....**72

ACKNOWLEDGEMENTS

I want to give my deepest thanks to my PhD advisor, Dr. William Sessa, for giving me the opportunity to be part of his research group . Dr. Sessa was a great mentor and one of the most brilliant, and humble people I have ever encountered. He constantly provided me with so much encouragement and guidance throughout my PhD years. His doors were always open for any question or concern. He was a huge support system for me in times when I experienced moments of self-doubt in my abilities to continue my research studies. I admired Dr. Sessa for his enthusiasm, his deep sense of curiosity and for taking his students' success personally, all of which were reflected in his mentorship philosophy. I had the privilege to know Dr. Sessa and work under his mentorship, and I hope I could follow his footsteps as I continue my scientific career.

I also want to deeply thank my collaborator, Dr. Ya Ha, whom I worked closely with during my third, fourth and fifth year of my PhD program. Dr. Ha was an incredible teacher, and I am hugely thankful for his time and efforts in teaching me all the theoretical and technical aspects of x-ray crystallography. He was always available whenever I needed him to explain a question or learn a certain research aspect. He deeply cared about my academic and personal growth as a scientist and to which I am grateful for. I really admired Dr. Ha's teaching style and had the honor to learn from his great mind.

I appreciate and thank my committee members: Dr. Karen Anderson, Dr. Ya Ha and Dr. Yong Xiong for their support and guidance during our annual meetings. They were incredibly supportive, encouraging and provided me with valuable suggestions. I am deeply honored to know and learn from each one of them.

When I think about how great my PhD experience was, the first person comes to my mind is Dr. Kariona Grabinska, a research scientist in the Sessa lab. I worked very closely with Dr. Grabinska during my PhD years since day one and I am deeply thankful for all the help she provided me to push my project forward. Dr. Grabinska is an incredible human being who never hesitated to help me with all she could or direct me to people who might know. It was simply enough to have one conversation with her to cheer me up on a difficult day. Her deep enthusiasm for science and devotion in teaching apprentice scientists is truly admired and much appreciated.

I want to greatly thank Rong Zhang, a lab technician in the Sessa lab, for providing me with her technical support during my third and fourth years. Rong was a great source of help when I needed to grow cells and purify protein. Her deep technical knowledge is hugely appreciated, and I am grateful for her help and support. I also want to thank my other lab members: Dr. Bo Tao for helping me collecting diffraction data for long hours, Dr. Nabil Boutagy for his constant support and help with my writing, Dr. Anamaria Gamez for her friendship and great encouragement, Dr. EonJoo Park, Dr. Victor Garcia, Dr. Wenping Zhou, Joseph Wayne Fowler and Dr. Sungwoon Lee for their kindness and support. I thank Diane Strumpf, our former administrative assistant, for facilitating the ordering process of chemicals and reagents and for her huge mental support. I also thank Roger Babbitt, a former manager in the Sessa lab, for his technical and instrumentation support. I am also grateful for Dr. Yvonne Gindt, my undergraduate advisor, for giving me the first opportunity to do research in her lab. She was a great mentor and played a key role in my decision-making process to pursue a PhD degree.

Lastly, I want to thank my family: my parents Dr. Husham Edani and Dr. Sulafa Edani, and my dearest sister and fellow scientist, Dina Edani, for their huge love and support throughout

my life. They are my role models of hard work, persistence, and success. I am profoundly grateful for all the sacrifices my parents made to ensure a great life for me and my sister. I will always appreciate all they have done, and I hope that dedicating this PhD dissertation to them is a small pay off. I am truly lucky to have my family by my side and be who I am today.

CHAPTER 1: Introduction

1.1 Isoprenoid biosynthesis

Isoprenoids constitutes the largest family of naturally occurring compounds produced by living organisms. They serve myriad biological functions such as: quinones used in electron transport chain, sterols serving as a structural component of biological membranes and a precursor of steroid hormones, photosynthetic pigments (carotenoids, retinoids, and side chain of chlorophyll), in protein prenylation important for subcellular targeting, plant hormones including gibberellins and abscisic acid, plant terpenoids (mono-, di- and sesqui-terpenes), and polyprenols such as dolichols which are employed as sugar carrier lipids during protein glycosylation (1-6). Despite their diverse roles, the basic structure of all isoprenoids is formed by the condensation of two C_5 precursors: isopentenyl diphosphate (IPP) and its isomer dimethylallyl diphosphate (DMAPP) (2). In most eukaryotes, archaea, and some eubacteria, IPP and DMAPP are synthesized via the mevalonate pathway (MVA), also known as the HMG-CoA reductase pathway (7). In contrast, most bacteria and chloroplasts of photosynthetic organisms utilize the methylerythritol phosphate (MEP) pathway to generate IPP and DMAPP (8).

Linear isoprenoids are formed by the condensation of an allylic diphosphate substrate with certain number of IPP (homoallylic substrate) units, catalyzed by prenyl chain elongating enzymes known as prenyltransferases (6). The newly synthesized products vary in their chain length from C_{10} to $C_{>10,000}$ (6, 9). With respect to the stereochemistry of the newly formed double bond of the product, prenyl-transferases are classified into two categories: *trans*-prenyltransferases (*trans*-PTases) and *cis*-prenyltransferases (*cis*-PTases) (2, 10, 11). Although both enzyme groups utilize similar substrates, biochemical and biophysical characterization of these enzymes revealed major differences in terms of their primary amino acid sequence, three-

dimensional (3D) structure, and molecular mechanism (6, 12, 13). In this work, however, I will focus on the structure and catalytic mechanism of *cis*-PTase enzymes.

1.2 *Cis*-prenyltransferase: enzymatic reaction and classification

cis-prenyltransferase (*cis*-PTase) plays a pivotal role in the synthesis of isoprenoids in the cis-configuration by catalyzing the sequential condensation of an allylic pyrophosphate primer with a variable number of isopentenyl pyrophosphates (IPP, C_5), resulting in the formation of a polyprenol pyrophosphate with *cis*-double bonds (6, 12, 14, 15). The most common type of *cis*-PTase catalyzes a "head-to-tail" condensation whereby the newly formed double bond is between C1' of the allylic substrate and C4 of the IPP molecule, thus generating linear isoprenoids (10, 16), (SI Appendix, Fig. S1). Recently, few studies have reported homologous of *cis*-PTase catalyzing an unusual "head-to-middle" condensation reaction in which a double bond is formed between C1' of the allylic primer and C2 of the IPP substrate, resulting in the synthesis of branched isoprenoids (10, 17, 18). Therefore, isoprenoids are the most structurally diverse, naturally occurring compounds with myriad biological functions in all living organisms (2, 6, 10). In eukaryotes, the *cis*-PTase localized to the endoplasmic reticulum (ER) is the first enzyme committed to dolichol phosphate (Dol-P) biosynthesis (15, 19-22), an obligate glycosyl carrier lipid crucial for protein N-glycosylation, O-mannosylation, C-mannosylation, and GPI anchor synthesis (2, 6, 23). Similarly, the bacterial *cis*-PTase, including the most common undecaprenol pyrophosphate synthase (UPPS), plays an essential role in maintaining cellular integrity by synthesizing UPP (11 C_5), a carrier lipid for *N*-acetylglucosamine-*N*-acetylmuramate pentapeptide moiety required for bacterial cell wall synthesis (24, 25). Therefore, UPPS serves as a target for the development of more effective antibiotics (24, 26-28).

Based on enzyme composition, *cis*-PTases can be either homodimeric or heteromeric enzymes (2, 10). The classification can be further extended to include product chain length in which the majority of homodimeric enzymes synthesize short-chain (2-5 C_5) or medium-chain (9-11 C_5) products whereas heteromeric enzymes tend to synthesize long-chain (14-24 C_5) or very-long-chain (> 2,000 C_5) products (2, 6). Many organisms including bacteria, some archaea, plants, and some protozoa such as *Giardia* and *Trypanosoma* possess a homodimeric *cis*-PTase assembly (2, 14, 29-36). Heteromeric enzymes, on the other hand, can be found in yeast, mammals, fungi, slime molds and some archaea and plants; these enzymes are mainly involved in the biosynthesis of long-chain dolichols required for dolichol-dependent protein glycosylation (2, 37-39). The well-known heteromeric *cis*-PTase synthesizing extensively long isoprenoids is rubber synthase (40, 41). Recently, studies on natural rubber biosynthesis have gained considerably increased attention from an industrial standpoint due to its unique physical properties and the high demand for sustainable rubber resources. Clearly, *cis*-PTases are diverse group of enzymes that synthesize wide range of precursors vital across all domains of life.

1.3 Evidence for the heteromeric organization of eukaryotic *cis*-PTase

The first eukaryotic genes encoding the putative *S.cerevisiae cis*-PTase proteins RER2 and SRT1 were identified two decades ago (15, 42, 43). Overexpressing either *RER2* or *SRT1* gene suppresses the phenotype of a *rer2* strain defective in yeast growth, protein sorting, *cis*-PTase activity and protein glycosylation (15). Subsequently, sequence homology analysis resulted in the identification of a cDNA encoding the human dehydrodolichyl diphosphate synthase (DHDDS) subunit (20, 22). Similar to *RER2* and *SRT1*, the human *DHDDS* complements growth defects, *cis*-PTase activity and restores normal protein glycosylation levels in the *rer2* mutant strain (22). Although DHDDS has no predicted trans-membrane domains, it is

membrane-associated (22). Furthermore, overexpression of DHDDS in mammalian cells results in a modest increase in *cis*-PTase activity from isolated microsomal fractions, indicating the requirement of an additional *cis*-PTase subunit (22). NgBR was first identified in the Sessa lab as a receptor that binds the amino terminus of Nogo-B (or reticulon 4B), a protein that is highly abundant in endothelial cells and vascular smooth muscle cells and plays an important role in adhesion and chemotaxis of endothelial cells (44). Initial studies on the cellular role of NgBR demonstrated an interaction between the C-terminus of NgBR and Niemann-Pick type C2 (NPC2), a lysosomal protein involved in the trafficking of LDL-derived cholesterol (45, 46). In addition, loss of NgBR using siRNA reduced the levels of NPC2 and induced accumulation of free cholesterol, a phenotype similar to NPC2 loss-of-function mutations (45). Furthermore, NgBR knockdown cells showed a remarkable decrease in *cis*-PTase activity, dolichol levels and protein N-glycosylation, suggesting a possible role in *cis*-PTase enzymatic function (46). Indeed, amino acid sequence analysis revealed a 44% sequence similarity between the C-terminus of NgBR and the homodimeric *cis*-PTase from *M.luteus* (46). Furthermore, co-immunoprecipitation studies established an interaction between the C-terminus of NgBR and DHDDS, indicating the presence of a heteromeric *cis*-PTase complex (46).

Genetic and biochemical studies from the Sessa group provided an unequivocal evidence for the heteromeric organization of *cis*-PTase in yeast and human. Studies in yeast demonstrated that a triple deletion yeast strain from *S.cerevisiae* lacking its three *cis*-PTase components, including *NUS1* (NgBR ortholog) and *RER2* and *SRT1* (DHDDS orthologs) was lethal, and survival of yeast cells was accomplished by expressing a homodimeric *cis*-PTase from *G.lamblia* (refer to method section for more details) (39). Similarly, viability of the triple deletion yeast strain was only possible by the co-expression of both NgBR and DHDDS but not individual

genes. These observations were further supported by a reverse-phase TLC analysis showing polyprenol formation occurring only in the presence of both *cis*-PTase components (39). In addition, in vitro-translation experiment combined with *cis*-PTase activity assay clearly demonstrated that only co-translation and not mixing of the two subunits reconstituted the activity of the complex (39). Subsequent work by other groups further bolstered the strict requirement of both subunits for *cis*-PTase activity and polyprenol synthesis in distantly related species. Using yeast two-hybrid screen and co-immunoprecipitation assays, *Brasher et al*.(37) demonstrated that a heteromeric *cis*-PTase from tomato required SICPT3 (DHDDS ortholog) and SICPTBP (NgBR ortholog) to complement growth defects and dolichol deficiency of yeast mutant lacking *RER2* gene. Similar results were reported by Epping et al. (40) whereby the interaction of rubber synthase components TbCPT1 (DHDDS ortholog)/TbRTA (NgBR ortholog) from Dandelion was confirmed by co-immunoprecipitation experiments. Moreover, expressing individual subunits failed to support cellular growth in the *S.cerevisiae* triple deletion strain (40). Yet in another study by Qu et al. (41), the plant *cis*-PTase complex from Lettuce was shown to consist of CPT3 (DHDDS ortholog) and CPTL2 (NgBR ortholog) using a yeast two-hybrid screen. In addition, only yeast microsomes containing CPT3/CPTL2 showed enhanced synthesis of *cis*-polyisoprenoids (41). Similar results were reported in a study by Kwon et al. (47) which demonstrated the requirement of both *cis*-PTase subunits CPT1 (DHDDS ortholog) and AtLEW1 (NgBR ortholog) in *A.thaliana* using yeast complementation and in-vitro activity assays. Recently, our group successfully isolated and biochemically characterized an archaeal, heteromeric *cis*-PTase from *M.acetovorans,* which consists of the two subunits MA3723 (DHDDS ortholog) and MA4402 (NgBR ortholog) (9). Similar to previous findings, both

subunits were necessary for the survival of the triple deletion yeast strain and optimal *cis*-PTase activity (9).

1.4 The molecular mechanism of heteromeric *cis*-PTase remains elusive

Our current mechanistic understanding of *cis*-PTase enzymes stems mainly from structural and biochemical studies on homodimeric enzymes which have been well characterized two decade ago. The first crystal structure reported for this enzyme group was from *M.lutues* UPP synthase (48). Subsequent crystal structures of other homodimeric *cis*-PTs revealed a similar structural fold in which each monomer consisted of six parallel β strands and seven α helices (28, 49-51). The enzymatic reaction takes place within a hydrophobic cavity composed of two α helices and two β strands (50, 52). Comprehensive structural and functional studies showed that most conserved residues involved in catalysis and substrate binding are located within the entrance of the cavity which is surrounded by positively charged residues to bind and stabilize the negatively charged pyrophosphate of the two substrates and product (50, 52, 53). In addition, previous fluorescence studies concerning the role of Mg^{2+} in substrate binding revealed that binding of the allylic substrate (i.e. FPP) is independent of Mg^{2+} while IPP binding only occurs in complex with Mg^{2+}(50). A highly conserved Aspartic acid (Asp26 in *E.coli* UPPs) within the active site was shown to coordinate with Mg^{2+} and play an important role in catalysis as suggested by the 1000-fold reduction in k_{cat} upon mutation to Alanine (54). The interior side of the cavity is surrounded by hydrophobic residues which can participate in binding the hydrophobic tail of the product; such assumption was supported by a crystal structure of *E.coli* UPPs in complex with Triton which is thought to mimic UPP, the product of the bacterial enzyme (52).

In contrast, the structure and molecular mechanism of heteromeric *cis*-PTase remains elusive due to their recent discovery. Identification of several heteromeric *cis*-PTs from different organisms revealed that DHDDS-like proteins retain most *cis*-PTase active site residues involved in catalysis and substrate binding (9). Nevertheless, purified DHDDS is only slightly active on its own (55). NgBR and its orthologs on the other hand seem to lack most of the functionally conserved residues except for a conserved C-terminal -RXG- motif, shared with homodimeric *cis*-PTases but not DHDDS orthologs (9). Both NgBR and DHDDS-like proteins retain the canonical dimeric interface region of homodimeric *cis*-PTase enzymes (9). Interestingly, NgBR harbors an N-terminal region that can bind to the ER membrane (46). Therefore, different roles have been assigned to NgBR-like proteins by various groups. A docking role was reported by Yamashita et al. (56), who recently described a three-component rubber synthase system from *Hevea brasiliensis* consisting of HRT1 (DHDDS ortholog), HRBP (NgBR ortholog) and a rubber elongation factor. Moreover, it was suggested in other studies that NgBR anchoring may activate DHDDS (57) or facilitate product release into the membrane (58). Although most NgBR orthologs are membrane anchored compared to the membrane-associated pattern of DHDDS, the anchoring role has been challenged by the following observations: First, a knockdown of NgBR showed no change in the relative abundance of DHDDS associated with isolated ER membrane fractions (46). Second, NgBR lacking its N-terminal domain (Δ85) still supports growth of a yeast triple strain when co-expressed with DHDDS (9). Lastly, a recently identified NgBR homolog from Archaea (MaUPPS-B) lacks the N-terminal domain containing the predicted membrane binding region yet was able to support *cis*-PTase activity and protein glycosylation (9). It is possible that the main role of NgBR is to stabilize the heteromeric complex; however,

recent functional studies from our group strongly suggest its additional role in *cis*-PTase enzymatic activity through its shared C-terminal -RXG- motif (9).

1.5 Genetic disorders associated with *cis*-PTase loss-of-function mutations

In the past few years, dolichol metabolism has received a considerable interest as more studies emerged demonstrating a clear relationship between defects in dolichol biosynthetic genes and numerous human diseases. More specifically, exome sequencing of patients with congenital disorders of glycosylation (CDG) type I has identified number of disease-causing mutations in both NgBR and DHDDS subunits (39, 59-63). A homozygous mutation (R290H) at the C-terminal -RXG- motif of NgBR was reported in a family of Roma origin (39). Individuals with this mutation exhibited a severe CDG type I phenotype with multi-organ symptoms including congenital scoliosis, refractory epilepsy, retinitis pigmentosa, microcephaly and severe neurological impairment (39). Biochemical characterization of R290H mutation by our group showed a marked reduction in *cis*-PTase activity as well as IPP binding with no influence on its interaction with DHDDS (9, 39). These data suggest a possible role for NgBR in catalysis and IPP binding through its C-terminal -RXG- motif (51, 64, 65). Another two homozygous mutations (K42E, T206A) in DHDDS were reported in individuals with a mild form of CDG whereby patients suffered from a nonsyndromic, autosomal recessive Retinitis Pigmentosa, commonly found among the Ashkenazi Jewish population (62, 63, 66). Interestingly, patients harboring either the $NgBR^{R290H}$ or $DHDDS^{K42E}$ homozygous mutations showed altered ratios of dolichol chain length in urine and plasma (39, 66). However, the physiological significance of this phenotype is still poorly understood. Yet another exome sequencing study recently reported several de novo heterozygous mutations in NgBR/DHDDS complex associated with neurological abnormalities in CDG. The symptoms lead to Developmental and Epileptic Encephalopathy

(DEE), a group of conditions characterized by re-occurrence of epilepsy and intellectual disability (ID) , electroencephalographic abnormalities and in few cases, early death (60, 67). Individuals carrying the de novo mutations displayed various neurological symptoms typical of DEE including epilepsy, seizures, tremors, ataxia and moderate to severe developmental delay (60). Moreover, micro-deletions within NgBR locus have been associated with pediatric epilepsy and congenital anomalies (68, 69). Finally, a recent exome sequencing study by Guo et.al, (70) identified de novo mutations in NgBR which might be relevant to Parkinson's disease pathogenesis, although it is uncertain whether these mutations affect *cis*-PTase activity.

1.6 NgBR regulation and cancer prognosis

In recent years, there has been a growing number of studies describing the correlation between NgBR expression and tumorigenesis. In the area of breast cancer research, it was shown that NgBR expression levels were elevated in breast cancer cells in relation to normal, non-transformed breast cells (71-73). More specifically, NgBR protein was highly expressed in estrogen receptor alpha (ERα)-positive/Her2-neggative breast cancer and was positively correlated with the expression of survivin, a well-known apoptosis inhibitor (72). In another study by Zhao et al. (74), NgBR knockdown was shown to reduce epithelial-mesenchymal transition (EMT), an essential process involved in breast cancer metastasis. Therefore, NgBR may play a role in the progression and metastasis of invasive ductal breast carcinoma. Several lines of evidence exist demonstrating an altered pattern of protein *O*- and *N*-glycosylation in cancer cells compared to normal cells (71, 75, 76). Given the essential role of NgBR as part of *cis*-PTase complex required for protein glycosylation, it might be reasonable to conclude that NgBR upregulation in tumorigenic cells occurs in response to the increasing demand for protein glycosylation. Moreover, it was previously shown that NgBR can interact with farnesylated Ras

and promote its accumulation to the plasma membrane, a crucial step required for the activation of epidermal growth factor (EGF) signaling pathway in breast cancer cells (77). In addition, NgBR overexpression was found to promote the activation of Ras-mediated EGF signaling, and Akt/ERK-mediated MDM2 phosphorylation, leading to the ubiquitination and degradation of p53 (78, 79). Such molecular mechanism is thought to explain the chemoresistance of ERα positive breast cancer cells to paclitaxel and tamoxifen (78, 79). A similar NgBR-Ras activation effect was observed in non-small cell carcinomas (NSCLC) cells (80, 81). According to these studies, NgBR knockdown was shown to inhibit EMT of NSCLC cells, whereas NgBR overexpression promoted Ras activation and its downstream MEK/ERK/Snail1 signaling pathway (81). Nevertheless, more studies are needed to fully illustrate whether NgBR-mediated Ras activation involves *cis*-PTase pathway or contribute to an independent role of NgBR in cancer progression and metastasis.

1.7 Thesis aims

Dolichol plays a crucial role as a gylcosyl carrier lipid required for proper protein glycosylation. Nevertheless, the steps leading to its biosynthesis remain poorly characterized. *Cis*-prenyltransferase (*cis*-PTase) is the first enzyme committed to the de novo biosynthesis of dolichols in eukaryotes (15, 19, 22). Recent studies by our group and others have already confirmed the heteromeric organization of eukaryotic *cis*-PTase enzyme, which consists of NgBR and DHDDS subunits in humans (37, 39-41, 46). In line with the significance of protein glycosylation for proper cellular function, mutations in both NgBR and DHDDS subunits have been associated with various clinical symptoms, ranging in severity from the mild retinitis pigmentosa to the fatal cases of congenital disorder of glycosylation (CDG type I) (39, 59-63, 70). Despite the growing clinical relevance of *cis*-PTase enzymes, a thorough investigation of heteromeric *cis*-PTases has been lacking due to their recent discovery. Towards this end, my thesis sought to gain an insight into the molecular mechanism of heteromeric *cis*-PTases through a structural-functional approach.

Thesis aim: Investigate the molecular mechanism of heteromeric cis-PTase enzymes *through the utilization of x-ray crystallography*

To gain a mechanistic understanding of heteromeric *cis*-PTase enzymes, I will determine the atomic structure of the human NgBR/DHDDS complex using x-ray crystallography technique. The structure will help shed light on the molecular determinants governing: 1) the heteromeric assembly of the two distantly related NgBR and DHDDS subunits to form a functional enzymatic complex; 2) the similarities and differences between the active site of heteromeric and homodimeric *cis*-PTase enzymes; 3) the mechanism underlying NgBR and DHDDS-related human diseases; 4) the role of membrane binding in enzyme activation; 5) the

mechanism by which heteromeric *cis*-PTase enzymes synthesize longer-chain polyprenols compared to homodimeric enzymes. Therefore, the structural study proposed herein will provide the first biophysical evidence for the interaction between NgBR and DHDDS subunits and will uncover the role of NgBR in the overall catalytic mechanism of heteromeric *cis*-PTase enzymes.

CHAPTER 2: The Crystal Structure of Human *cis*-PTase (NgBR/DHDDS) Complex Reveals Novel Insights into the Molecular Mechanism of Heteromeric Enzymes

2.1 Introduction

Until now, all studies concerning the structure and catalytic mechanism of *cis*-PTase have been limited to homodimeric enzymes. In contrast, our mechanistic understanding of prenyl chain elongation by heteromeric enzymes remains elusive. Previous biochemical studies from our lab confirmed the heteromeric organization of the human *cis*-PTase, which consists of NgBR and DHDDS subunits (39, 46). Unlike homodimeric *cis*-PTases which synthesize short and medium-chain length products (e.g., *E.coli* UPPS; 11 isoprene units); human *cis*-PTase catalyzes the condensation of sixteen IPP units with a single farnesyl pyrophosphate (FPP) molecule, generating a long-chain polyprenol diphosphate (19 isoprene units) (SI appendix, Fig. S1) (2) . Once synthesized, the polyprenol diphosphate is then dephosphorylated by an unknown phosphatase, generating polyprenol. The α-isoprene unit of the polyprenol is subsequently reduced by an NADPH-dependent polyprenol reductase, resulting in the formation of dolichol. The last step involves phosphorylating the dolichol by a dolichol kinase to form dolichol phosphate, the glycosyl carrier lipid required for various types of protein glycosylation in the lumen of endoplasmic reticulum (2, 6, 23). The essential role of *cis*-PTase in dolichol synthesis was demonstrated using yeast, mice, and zebrafish as genetic models. Notably, a global knockout of NgBR in mice (39) and endothelial specific knockout of NgBR (82) leads to embryonic lethality due to defects in vascular development. Similarly, NgBR knockdown in zebrafish embryos shows defects in intersomitic vessel sprouting (83). In addition, deletion of yeast *S.cerevisiae cis*-PTase components including Rer2/Srt1(DHDDS orthologs) and Nus1 (NgBR ortholog) fails to support growth of yeast cells (30, 39). Moreover, in vitro studies using

endothelial-specific NgBR knockdown cells show a marked reduction in cell proliferation and an increase in apoptosis, mainly due to the hypoglycosylation of essential endothelial cell proteins such as VEGFR2 (82).

Several lines of evidence exist supporting the requirement of both NgBR and DHDDS and their orthologs for a functional *cis*-PTase enzyme (9, 37, 39-41, 46, 47). Nevertheless, the specific contribution of each subunit to the overall catalytic mechanism is unclear. Intriguingly, DHDDS is a soluble protein yet localizes to the ER membrane (22). Additionally, DHDDS shares a high sequence homology (up to 50% sequence similarity) with homodimeric *cis*-PTases, thus retaining most active site residues involved in catalysis and substrate binding (9). In contrast, NgBR can be divided into two domains: An N-terminal domain which exhibits a membrane-binding region, and a C-terminal domain that seems to share a low sequence identity with homodimeric *cis*-PTases by lacking most active site residues (9, 44). However, our group has recently identified a conserved -RXG- motif at the very C-terminus of NgBR; the motif is shared with homodimeric *cis*-PTases but not DHDDS and its orthologs (9). A functional analysis of the C-terminal -RXG- motif revealed its critical role in catalysis and binding of the IPP substrate (9); thus, suggesting a catalytic role for the NgBR subunit. Recently, the structure of *cis*-PTase domain of Nus1 (NgBR ortholog from yeast) was reported (84); surprisingly, Nus1 adapts a structural fold similar to that of homodimeric *cis*-PTase enzymes. Additionally, sequence alignment studies revealed both NgBR and DHDDS to maintain the canonical interface region commonly found in homodimeric enzymes (9). Nevertheless, a more thorough investigation is needed to elucidate the dimeric interaction and the real contribution of both subunits to the overall molecular mechanism of heteromeric *cis*-PTases. Towards this end, I developed a bacterial system for the co-expression and purification of the human NgBR/DHDDS

complex. Next, I successfully co-crystallized the heteromeric enzyme in complex with Mg^{2+} ion and IPP substrate at 2.3 Å. The structural-functional analysis unveiled novel features that were not previously predicted based on the structures of homodimeric enzymes. These features include a unique C-terminal domain on DHDDS that seems to contribute to the heterodimerization of the complex, a novel N-terminal membrane sensor on DHDDS that is critical for membrane activation, and a unique structural feature within the hydrophobic cavity of DHDDS that plays a role in product chain elongation. In addition, the structure confirmed the involvement of NgBR in the overall catalytic mechanism of *cis*-PTase and provided a mechanistic insight into the loss of function mutations associated with CDG. Therefore, NgBR/DHDDS complex structure sheds light on different molecular aspects of heteromeric *cis*-PTase enzymes and provides a model for the product chain elongation mechanism.

2.2 Materials and Methods

Materials

Unless otherwise stated, all reagents were of analytical grade and purchased from Sigma-Aldrich, Thermo Fisher Scientific, and Zymo Research (Irvine, CA). Restriction enzymes were from New England Biolabs (Ipswich, MA). [1-^{14}C] IPP (50 mCi/mmol) was purchased from American Radiolabeled Chemicals (St. Luis, MO). Reverse phase thin layer chromatography (RP18-HTLC) plates were from MilliporeSigma (cat# 1.51161.0001). Primary antibodies used in this study include Anti-HA High Affinity antibody (Roche, 11867423001) and Monoclonal anti-Flag M2 antibody (Sigma, F3165). HiFi DNA Assembly method (NEBuilder®, NEB) was used to construct expression vectors and perform site-directed mutagenesis.

Cloning and Purification of NgBR/DHDDS Complex

To express His-SUMO-NgBR$^{79\text{-}293}$ and untagged, full length DHDDS (1-333) in bacteria, His-SUMO and NgBR overlapping PCR fragments were first assembled into pRSF-DUET1 vector cut with NdeI/XhoI restriction enzymes. DHDDS PCR fragment was then assembled into pRSF-DUET1-HIS-SUMO-NgBR cut with NcoI/NotI. The Recombinant NgBR/DHDDS complex was expressed in *Escherichia coli* Rosetta (DE3) cells (Novagen) and induced with 0.7 mM IPTG (OD_{600} 0.6) overnight at 18 ºC. Cells were harvested and then resuspended in lysis buffer containing 20 mM Tris-HCl pH 8.0, 500 mM NaCl, 20 mM imidazole, 10% glycerol, 0.5% triton X-100 and 2 mM 2-Mercaptoethanol, cOmplete protease inhibitors (Roche), lysozyme (100 μg/ml) and DNase I (10 μg/ml). Three cycles of freeze/thaw were conducted using ethanol/dry ice bath and cells were sonicated in 50 ml falcon tube for 2 minutes total. The samples were clarified by centrifugation at 20,000 rpm for 1 hour at 4 ºC. Supernatant was then

applied to a 1 ml HisTrap (GE Healthcare) nickel affinity column, and the protein was eluted with 6 ml lysis buffer containing 400 mM imidazole. The sample was then applied to size exclusion column (Superdex 200, GE Healthcare) equilibrated with buffer containing (50 mM Tris-HCl pH 8.0, 150 mM NaCl, 1 mM $MgCl_2$ and 2 mM TCEP). Fractions containing protein complex were collected and subjected to cleavage with SUMO protease overnight at 4ºC to remove the His-SUMO tag. The cleaved protein was then re-applied to a HisTrap column and the flow-through was collected. Protein sample was then passed through another size exclusion column equilibrated with 50 mM Tris-HCl pH 8.0, 150 mM NaCl, 2.5 mM $MgCl_2$ and 2 mM TCEP. Fractions were collected and analyzed by 12% SDS-PAGE gel.

Crystallization, Data Collection and Structural Determination

The purified protein was concentrated to 3.2 mg/ml and incubated with 3.3 mM IPP (sigma) on ice for 2 hours. Crystallization screening was performed using the sitting-drop vapor diffusion method, and an initial hit was obtained from PEG screen (Hampton Research). Crystallization was optimized by grid screening and the best crystals were obtained by mixing 1 µl protein solution with 1 µl reservoir solution consisting of 0.1 M Bicine (pH 8.5), 10% v/v 2-propanol, 22% PEG 1500. Crystals appeared within 2 days and grew to maximum size within one week at room temperature. Crystals were cryoprotected with the reservoir solution supplemented with 20% glycerol and flash frozen in liquid nitrogen. Diffraction Data were collected on beamline 24-ID-E of the Advanced Photon Source at Argonne National Laboratory and processed using *HKL2000* (85). Although individual reflections up to 2.2 Å resolution could be observed, after merging, $CC_{1/2}$ quickly fell off beyond 2.3 Å. The structure of the complex was determined by molecular replacement and refined to 2.3 Å resolution using CCP4i

(supplementary Table 1) (86). The *E. coli* UPPs (PDB entry 1X06) and *S. cerevisiae* NUS1 (PDB entry 6JCN) were used as search probes for the DHDDS and NgBR subunits, respectively. Model building were performed using *Coot* (87).

cis-PTase activity of NgBR/DHDDS

The steady state activity of purified NgBR/DHDDS complex was assayed as before with minor modifications (9). Briefly, a standard incubation mixture contained, in a final volume of 25 µl, 100 µM [1-^{14}C] IPP, 20µM FPP, 50 mM Tris-HCl pH 8.0, 1 mM $MgCl_2$, 10 mM KF, 20 mM 2-mercaptoethanol, 1 mg/ml BSA ,1 % Phosphatidylinositol and 100 ng of purified enzyme. The mixture was incubated for 1 hour at 37 ºC and product was extracted with chloroform:methanol (3:2), followed by washing three times with 1/5 volume of 10 mM EDTA in 0.9% NaCl. In order to determine the chain length of the cis-PTase products, polyprenol diphosphates were chemically dephosphorylated by incubation of the lipids at 90° in 1 *N* HCl for 1 hr. Dephosphorylated prenols were extracted three times with two volumes of hexane. The organic fraction was washed with 1/3 volume of water, hexane was evaporated under stream of nitrogen and lipids were loaded onto HPTLC RP-18 precoated plates and run in acetone containing 50 mM H_3PO_4. The plates were exposed to film to visualize the products of IPP incorporation. As an internal and external standards Geranylgeraniol (Echelon Biosciences), Undecaprenol and Polyprenol 19 (*Institute of Biochemistry and Biophysics*, PAS the *Collection* of Polyprenols) and Prenols mixture (13-21) (Avanti Polar Lipids) were used. Prenol standards were visualized by exposing the TLC plate to iodine vapor.

Limited Proteolysis

20 ul of 0.2 mg/ml of purified NgBR/DHDDS enzyme was incubated with 5 ul of a protease including thermolysin (S*igma*), proteinase k (S*igma*) and trypsin (S*igma*) at different concentrations (0.005, 0.01, 0.02, 0.04, 0.08, 0.16 mg/ml). The reaction mixture was incubated at room temperature for 30 minutes and stopped with SDS buffer containing 5.2 mM PMSF and 5.2 mM EDTA. Samples were boiled for 5 minutes and analyzed by12% SDS-PAGE gel.

Co-Immunoprecipitation

HEK293T cell was transfected using lipofectamine 2000 (Invitrogen) according to the manufacturer's protocol and harvested 48 hrs after transfection. Cells were collected and lysed in IP buffer (IP buffer: 50mM HEPES, 150mM NaCl, 1mM EDTA, 1% Triton X-100, Complete Protease Inhibitors (Roche)). Lysates were cleared by centrifugation at 12000 rpm for 10 min and 10µl of anti-Flag M2 magnetic beads (Sigma) was used to pulldown the Flag-tagged protein from 0.5-1 mg of cell lysate. After incubation for 2 hours at 4˚C, magnetic beads were washed with IP buffer, resuspended in 2X Laemmli sample buffer and boiled for 5 min before western blot analysis.

Yeast Complementation Assay

For yeast complementation analysis of *cis*-PTase, *S. cerevisiae* strains KG405 (*nus1*Δ *rer2*Δ *srt1*Δ), carrying the *Glcis*-PTase encoding gene on a plasmid with a *URA3* marker was used (39). To phenotypically analyze human *cis*-PTase mutants, strain KG405 was transformed with vectors pKG-GW1 carrying DHDDS variants (leucine selection) and pKG-GW2 carrying NgBR variants (methionine selection) in combination or empty vectors as negative control. Transformed yeast cells were grown overnight at 30 °C in synthetic defined

medium or lacking uracil, methionine, and leucine were streaked onto synthetic defined medium containing all amino acids, nucleotide supplements, and 1% (w/v) 5-FOA (Zymo Research) and onto YPD plates. The plates were incubated for up to 5 days at 30 °C. Colonies growing on the 5-FOA plates were streaked on synthetic defined medium lacking uracil and incubated at 30 °C for 3 days to verify the loss of the pNEV-Gl*cis*-PTase plasmid. Yeast strain KG405 and its derivative carrying NgBR/DHDDS complex were cultured in 2% (w/v) Bacto peptone and 1% (w/v) yeast extract supplemented with 2% glucose (w/v) (YPD). Synthetic minimal media were made of 0.67% (w/v) yeast nitrogen base and 2% (w/v) supplemented with auxotrophic requirements. For solid medium, agar (BD Biosciences, Sparks, MD) was added at a 2% (w/v) final concentration. Yeast cells were transformed using the Frozen-EZ yeast transformation II kit (Zymo Research).

HPLC Analysis

To estimate the chain length of dolichols produced by EKE deletion mutant, total lipids from 3 g of yeast cells grown overnight till late logarithmic phase of growth (OD 3-4) were extracted by the modified Folch method. Lipids extracted from yeast cells were hydrolyzed in hydrolytic solution containing toluene/7.5% KOH/95% ethanol (20:17:3, v/v/v) for 1h at 90°C. Nonsaponifiable lipids were then extracted four times with hexane, purified on silica gel 60 columns using isocratic elution with 10% diethyl ether in hexane, evaporated to dryness in a stream of nitrogen and dissolved in isopropanol. Extracts were analyzed by HPLC using a Waters dual-pump HPLC device coupled with a Waters Photodiode Array Detector (spectrum range: 210 - 400 nm) and ZORBAX XDB-C18 (4.6 × 75 mm, 3.5 μm) reversed-phase column (Agilent, USA). Polyisoprenoids were eluted using the solvent mixtures A - methanol/water, 9:1

(v/v) and B - methanol/isopropanol/hexane, 2:1:1 (v/v/v) combined as follows from 0% B to 75% B in 20 min, from 75% B to 90% B in 5 min, from 90% B to 100% B in 2 min, 100% B maintained for 11 min, then from 100% B to 0% B in 1min at a flow rate of 1.5 mL/min. The chain length and identity of lipids were confirmed by comparison with external standards of a polyprenol (Pren-10 – Pren-24) and dolichol (Dol-17 – Dol-23) mixtures.

2.3 Results

2.3.1 The core catalytic domain of NgBR/DHDDS complex

Previous SAXS analysis and circular dichroism studies by Holcomb et.al (88) showed a globularly folded protein when an NgBR construct devoid of its N-terminal region (1-78) was expressed and purified from bacterial cells. Accordingly, I co-expressed and purified a polyHis and SUMO-tagged NgBR (79-293) with full-length, untagged human DHDDS (1-333) using bacterial *E.coli* cells (Fig. 2.1A). The system yielded a highly pure, monodisperse protein in milligram quantities that are suitable for structural studies (Fig. 2.1B). Interestingly, upon careful examination of the size exclusion chromatogram, the protein complex seemed to elute at a volume that is higher than its expected molecular weight (~ 70 KDa). Further investigation using size-exclusion chromatography multi-angle light-scattering (SEC-MALS) revealed similar results, whereby the estimated molecular weight of the complex was ~ 120 KDa, corresponding to the size of a tetramer. Although only a dimeric form of the complex was crystallized (see below), it would be interesting to determine whether the higher oligomerization state of the protein complex observed in solution is an artifact of the purification strategy employed or has any physiological relevance. Next, I measured the enzymatic activity of the purified complex using radioactive [1-^{14}C] IPP substrate and cold FPP at steady-state conditions. The truncated complex exhibited full enzymatic activity similar to that of the full-length protein complex previously purified from mammalian Expi 293 cells (9). Furthermore, previous work from our lab demonstrated the requirement of phospholipids such as phophotidylinositol (PI) to potently stimulate the activity of purified NgBR/DHDDS enzyme (9). Accordingly, measuring protein stimulation by PI showed no difference between the truncated and the full-length protein complex (Fig. 2.1C). These results further support the notion that the N-terminal domain of

NgBR, which harbors a predicted membrane-binding region, is not required for the activity of the complex. Moreover, removing the N-terminal region of NgBR did not alter the range or relative abundance of the polyprenol pyrophosphate, the reaction product, when analyzed by reverse phase thin layer chromatography (see below).

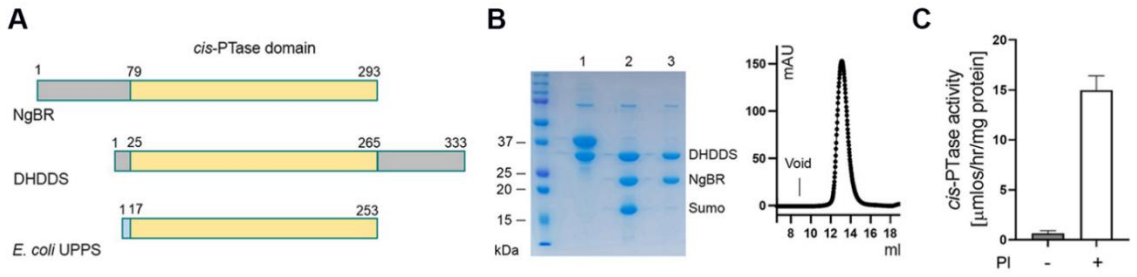

Figure 2.1 The catalytic core domain of human *cis*-PTase.

(A) Comparing the domain structure of NgBR, DHDDS and *E.coli* UPPS. The *cis*-PTase domain is colored yellow; N- and C-terminus of NgBR and DHDDS, gray; N-terminus of *E.coli* UPPS, blue.
(B) Purification of NgBR/DHDDS complex. Left Panel: Coomassie-stained SDS/PAGE showing purification steps. Lane 1**:** uncleaved 6HIS-SUMO-NgBR/DHDDS complex, Lane 2: cleaved NgBR/DHDDS complex and SUMO, Lane 3**:** NgBR/DHDDS complex after removing SUMO. Right panel, Size exclusion chromatography profile of the purified complex after cleavage with SUMO protease.
(C) Stimulation of *cis*-PTase activity of NgBR/DHDDS complex by phosphatidylinositol (PI). The values are means ±S.D. of eight independent measurements from two independent purifications.

2.3.2 Overall structure of the heteromeric complex

To better understand the molecular mechanism of heteromeric *cis*-PTases, I sought to determine the structure of NgBR/DHDDS complex using x-ray crystallography. The complex was successfully crystallized at 2.3 Å, in the presence of Mg^{2+} and IPP substrate using the sitting-drop vapor diffusion method. The crystal belongs to the space group R32, and the asymmetric unit contains a single NgBR/DHDDS heterodimer. The structure was determined by molecular replacement using *E.coli* UPPS (PDB entry 1X06) and *S.cerevisiae* Nus1 (PDB entry 6JCN) as search probes for DHDDS and NgBR, respectively (Fig 2.2A; SI appendix, Table S1) (50, 84). The structure revealed many unique features that were not previously observed in the search probes (SI appendix, Fig. S2-6). As shown in the structure, NgBR is composed of seven α-helices and six β-strands compared to nine α-helices and six β-strands in the DHDDS subunit. The superposition of DHDDS with *E.coli* UPPS structure showed C_α RMSD of 1.2 Å, and 1.8 Å for NgBR and Nus1 structures. Interestingly, DHDDS possesses a novel N-terminal region (residues 1-24) consisting of α-helix (α_0) and a random coil, which extends into the hydrophobic tunnel of DHDDS. Additionally, the C-terminal domain of DHDDS encompasses a unique pair of long α-helices (residues 251-333); the two helices are stabilized against each other by a salt bridge formed between D273 and R306 as well as several interactions with residues from both subunits; thus, contributing to the heteromeric interface of the complex. Similarly, NgBR structure revealed a novel N-terminal α-helix (residues 82-93) and a C-terminal segment (residues 286-293) which contains the catalytically conserved -RXG- motif. The two outermost β-strands (βC and βC') previously observed in the Nus1 structure are disordered (residues 230-244; SI appendix, Fig. S4). Strikingly, the peptide segment following the β-strands forms a new helix (α4, residues 179-186) and partially covers the hydrophobic cavity between α2 and α3,

which was once proposed to constitute the binding site for farnesylated Ras (77). Furthermore, a major difference exists between the architecture of the hydrophobic cavity of NgBR and other *cis*-PTases. In DHDDS as well as other UPPS structures, the two helices (α-helix 2 and 3) forming the hydrophobic cavity, are organized in a parallel fashion, thereby allowing for the chain elongation process (SI appendix, Fig. S5). In NgBR, however, α-helix 3 is much shorter, and directly associates with α-helix 2, leading to the collapse of the hydrophobic cavity. Such unique feature might account for the inability of NgBR to participate in the chain elongation process.

The crystal structure supports earlier notion that both NgBR and DHDDS subunits are required for enzymatic stability (39, 46). The dimeric interface of the complex resembles that of bacterial UPPS enzymes as well as yeast Nus1homodimer, burying an average of 2,029 $Å^2$ surface area (SI appendix, Fig. S7) (50, 84). In addition to the canonical interface region, the C-terminus of DHDDS wraps around the protein complex and makes additional contacts with NgBR, further contributing to the overall stability of the complex. This observation is in contrast with a recent modeling study demonstrating the DHDDS's C-terminal domain folding outside the core catalytic domain (55). To assess the nature of interaction between NgBR and DHDDS subunits, I conducted limited proteolysis studies on the purified complex using different types of proteases including thermolysin, proteinase k and trypsin. Under all conditions, a common theme was observed whereby NgBR cleavage occurred prior to that of DHDDS, thus supporting the stabilizing effect between these two subunits (Fig 2.2B; SI appendix, Fig. S8). To further test the heteromeric interface, co-immunoprecipitation experiments were conducted in HEK293T cells expressing the protein complex with several point mutations at the interface region. As shown in Fig 2.2C (and in SI appendix, Fig. S9), most of these mutations weakened binding between

NgBR and DHDDS, owing to their essential role in maintaining the integrity of the complex. Given the unique architecture of DHDDS's C-terminal region observed in the structure, I sought to investigate the contribution of this region using a genetic approach. Briefly, a triple deletion yeast strain devoid from its *cis*-PTase components (*rer2*Δ, *srt1*Δ, *nus1*Δ) and expressing a homodimeric *cis-PTase* from *G.lamblia* (39) was transformed with a complex containing different DHDDS modification and evaluated for phenotypic growth. These modifications included two DHDDS truncations (Δ256, Δ289) where part of α7 and the entire α8 helix were deleted, and a triple mutant (R306A/F313A/L317A), predicted to disrupt packing of the two C-terminal helices based on the structure (SI appendix, Fig. S3B). Both deletion mutants failed to support growth of yeast cells, whereas the triple mutant delayed growth (Fig 2.2D). Therefore, these data further support the essential role of DHDDS's C-terminal region and roles out the possibility of its uniquely folded structure as an artifact of crystallization.

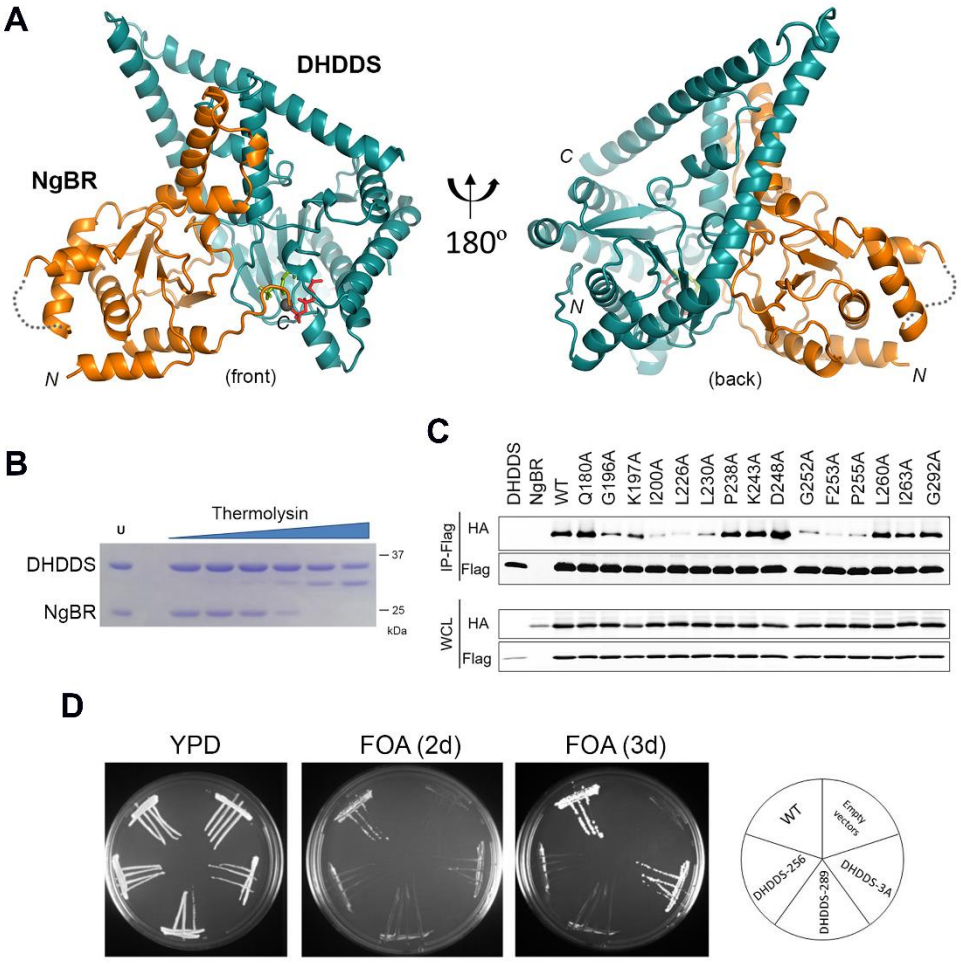

Figure 2.2 The overall structure of NgBR/DHDDS heterodimer.

(A) Ribbon diagrams showing the front and back of the heteromeric complex. NgBR is colored in orange and DHDDS is colored in deep teal. Mg^{2+} ion is shown as a gray sphere, IPP molecules occupying S1 and S2 sites are shown in red and green, respectively.
(B) Limited proteolysis of the core domain was performed by incubating the protein with increasing amounts of thermolysin (0.005, 0.01, 0.02, 0.04, 0.08, 0.16 mg/ml). Untreated protein sample is denoted as (U). In this gel, thermolysin co-migrates with the full-length DHDDS.
(C) Co-immunoprecipitation of NgBR/DHDDS mutations introduced at the complex interface. HEK293T cells were co-transfected with NgBR-HA and Flag-DHDDS cDNAs; cells were lysed 48 hours post-transfection and immunoprecipitation performed using anti-flag magnetic beads. The lysate was analyzed by western blotting.
(D) Characterization of *cis*-PTase mutants in the C-terminal region of DHDDS using yeast complementation assay. The *nus1*Δ *rer2*Δ *srt1*Δ deletion strain expressing *G. lamblia cis*-PTase from *URA3* plasmid was co-transformed with *MET15* bearing wildtype (WT) NgBR and the *LEU2* plasmid bearing either WT or mutant variants of DHDDS at the C-terminus. Three variants were analyzed including a triple mutation (3A) corresponding to R306A, F313, L317 and two DHDDS

truncation Δ256 and Δ289. The cells were streaked onto complete plates (YPD) or synthetic complete medium containing 1% FOA. The Ura3 protein, which is expressed from the *URA3* marker converts FOA to toxic 5-fluorouracil, forcing the cells to lose the *G. lamblia cis*-PTase plasmid. Cell growth was monitored over time to assess phenotypic differences.

2.3.3 The active site of NgBR/DHDDS complex

Unlike homodimeric *cis*-PTases which possess two active sites, one per monomer (48-51), heteromeric *cis*-PTase contains one active site, mainly located on the DHDDS subunit. As mentioned earlier, DHDDS harbors most critical residues involved in catalysis including the strictly conserved Asp acid (Asp 34 in DHDDS) as well as those required for binding of the allylic (i.e. FPP) and homoallylic (IPP) substrates, therefore resembling the active site of a homodimeric enzyme. Although the overall structural fold of NgBR, and its yeast homolog Nus1, is similar to that of DHDDS and members of the homodimeric *cis*-PTase family, they lack main catalytic residues and are unable to catalyze the reaction due to their distorted "active site". However, our recent sequence alignment studies revealed the presence of a conserved -RXG- motif at the C-terminus of NgBR and homodimeric *cis*-PTases but not DHDDS and its orthologs (9). Moreover, kinetic studies on the purified WT and -RXG- motif mutants showed a clear effect on catalysis and substrate binding. Specifically, a functional analysis of R290H, a disease mutation associated with fetal CDG type I case, showed ~ 4-fold reduction in k_{cat} and up to 2-fold increase in K_m for IPP (9). Additionally, substituting G292 with Ala reduced the enzymatic activity to a greater extent with k_{cat} that is 10-fold lower than that of WT enzyme and K_m for IPP that is 5-fold higher (9). Collectively, these results strongly support a functional role of NgBR in the overall catalytic mechanism.

The previously reported crystal structure of Nus1homodimer could not resolve the C-terminal -RXG- motif region (84). In contrast, our refined structure shows clear electron densities, allowing us to model the entire C-terminal region of NgBR, along with two IPP molecules: IPP1 molecule occupying the allylic substrate binding site S1, and IPP2 occupying the homoallylic binding site S2, as well as a bridging Mg^{2+} ion (Fig 2.3A; SI appendix, Fig. S2B,

S6 and S10). Strikingly, the C-terminus of NgBR traverses the dimeric interface which allows for the complementation of the active site (Fig 2.3B). As shown in the structure, the C-terminus makes number of unique interactions with the IPP substrate as well as residues from DHDDS subunit. The main chain amide group of Leu-291 and Gly-292 of the -RXG- motif forms hydrogen bonds with the β-phosphate group of the homoallylic IPP substrate, while the side chain of Arg-290 mainly interacts with a water molecule that coordinates with the Mg^{2+} ion. The presence of a Gly within the -RXG- motif is essential by allowing this peptide to make a tight turn over IPP2 and further stabilizes the turn through a Hydrogen bond formed with the conserved Arg-85 of DHDDS, which is involved in coordination with the pyrophosphate moiety of the allylic substrate. Therefore, the structure provides a mechanistic insight into the molecular role of the conserved -RXG- motif in conjunction with our previous functional studies.

Notably, the architecture of the allylic S1 binding site is highly conserved within the *cis*-PTase family (SI appendix, Fig. S11). Although the electron density corresponding to the hydrophobic tail of IPP1 was weak, we were confident in our modeling strategy employed whereby the prenyl tail extends into the hydrophobic tunnel to accommodate the elongated product (Fig 2.3A). In contrast to the S1 site, comparing S2 site of many crystal structures revealed some discrepancies, mainly concerning the arrangement of the C-terminal -RXG- motif (SI appendix, Fig. S12). In most cases, structures with a disordered -RXG- motif had poorer occupancy of the S2 site or misplaced pyrophosphate groups. In contrast, the S2 site in our current structure was occupied with the homoallylic IPP2 molecule and we were able to model it with great certainty. As shown in the structure, the pyrophosphate group of IPP2 is stabilized by number of interactions with DHDDS residues including the 3 highly conserved Arg residues (Arg-85, Arg-205, Arg-211), and a conserved Ser (Ser-213). The S2 site is sealed by the

extended -RXG- motif from NgBR, which makes additional contacts with the pyrophosphate moiety of IPP2 substrate. The S1 and S2 sites are bridged by the catalytically important Mg^{2+} ion required for hydrolysis of the allylic pyrophosphate group (50). The Mg^{2+} ion is coordinated by the pyrophosphate moieties of the two substrates, the strictly conserved Aspartic acid (Asp-34 in DHDDS) and two water molecules. Finally, previous work on homodimeric *cis*-PTases demonstrated the requirement of a base, most likely an Asparagine residue (Asn-74 in *E.coli* UPPS) to abstract a proton from C2 of IPP upon forming the new double bond (50, 89). Similarly, our structure shows Asn-82 in DHDDS subunit positioned within close proximity to C2 of IPP, thus serving the same proposed role during catalysis. Clearly, the structural similarities described above further suggest a common catalytic mechanism shared between homodimeric and heteromeric *cis*-PTase enzymes.

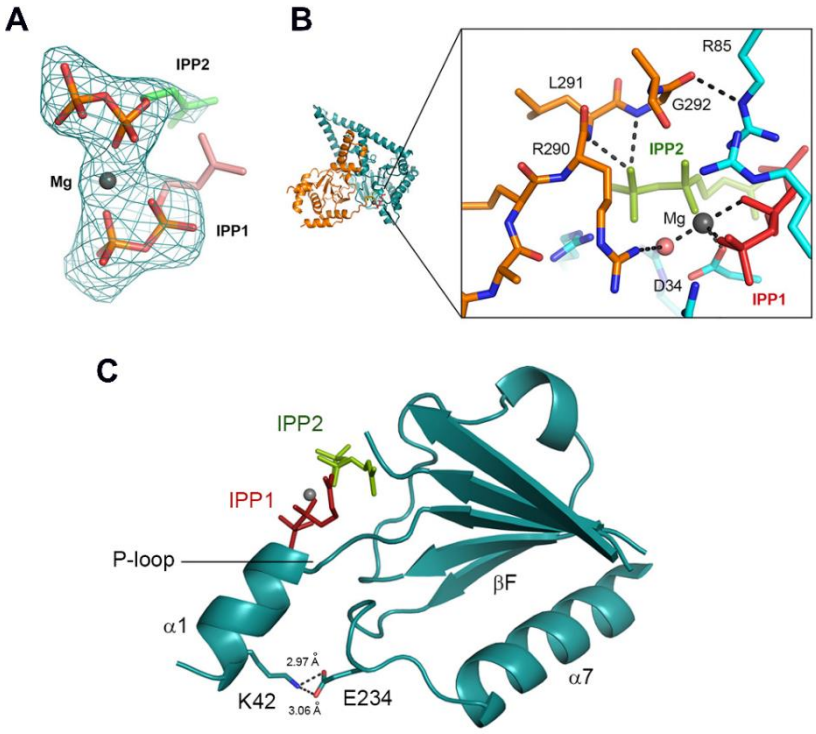

Figure 2.3 The active site of the NgBR/DHDDS complex.

(A) Omit difference map, countered at 3.0 σ level, showing the two IPP molecules and Mg^{2+} ion bound at the active site. IPP1 is assigned to IPP molecule bound at S1 site, and IPP2 to that at S2 site. The oxygen atoms are colored red and phosphorus atoms are colored orange. The carbon atoms of IPP1 are colored salmon and those of IPP2 are in green.
(B) Detailed view of the -RXG- motif and the active site. The carbon atoms of NgBR -RXG- motif residues are colored orange and labeled, and those for DHDDS are colored cyan. Nitrogen atoms are colored blue and oxygen atoms are colored red. IPP1 and IPP2 are colored red and green, respectively. Mg^{2+} is shown as a gray sphere, and its co-ordination is indicated by the dashed lines. A coordinating water molecule is shown as red sphere.
(C) The K42E retinitis pigmentosa mutation in DHDDS. A cartoon representation indicating the locations of Lys-42 and Glu-234 relative to the P-loop and bound substrates. DHDDS is colored in deep teal, IPP1 in red, IPP2 in green and Mg^{2+} is shown as a gray sphere.

2.3.4 Mapping disease mutations associated with the active site of NgBR/DHDDS complex

Mutations on both NgBR and DHDDS subunits have been linked to various clinical phenotypes, yet the molecular mechanism underlying their pathogenicity remains unclear. Therefore, our solved structure provides the first mechanistic insight into these mutations. Notably, the majority of CDG-causing mutations cluster around the active site of the complex and are directly involved in catalysis and substrate binding (SI appendix, Fig. S13A). Specifically, DHDDS mutations R37H and R38H associated with DEE are localized within the S1 site; the two Arg residues make direct contact with the pyrophosphate moiety of IPP1 or the allylic substrate. Similarly, another DEE mutation, R211Q, localizes within the S2 site and is directly involved in binding the pyrophosphate group of IPP2 or the homoallylic substrate. Finally, the NgBR R290H mutation associated with severe CDG phenotype, is localized within the -RXG- motif whereby R290 makes direct interaction with a water molecule which coordinates with Mg^{2+} ion. In addition to the above mutations, the structure also allowed for a detailed analysis of the two mutations associated with retinitis pigmentosa, namely T206A and K4E2, located on the DHDDS subunit. Although uncharacterized biochemically, T206A could directly perturb the active site since the Thr hydroxyl group is involved in hydrogen bonding with the backbone amide and carbonyl of the highly conserved, and catalytically essential Asp-34 (SI appendix, Fig. S13B, (65)). Unlike T206A, the homozygous K42E mutation, which affects ~ 17 % of Ashkenazi Jewish patients diagnosed with autosomal recessive retinitis pigmentosa (63, 90), does not directly interact with the substrate or active site residues. Previous predictions on the structural role of K42 residue were misleading since they were based on the crystal structure of UPPS enzymes. For instance, in the *E.coli* UPPS structure, K34, corresponding to K42 in DHDDS, is exposed to solvent and does not interact with any other

residue that could explain the mutation pathogenicity. However, our refined structure revealed a salt bridge formed between K42 and a highly conserved E234 (Fig 2.3C); this interaction is equivalent to that between W31 and D223 in *E.coli* UPPS. Therefore, K42E mutation will result in a repulsive effect that could perturb the short helix (α1) containing K42 residue. Since this helical region along with the proceeding P-loop are involved in FPP binding, this analysis further supports previous functional studies on K42E mutation which showed a reduction in K_{cat} and an increase in K_m for FPP but not IPP substrate (9).

In addition to the published mutations described above, our structure enabled for the characterization of series of de novo mutations on the DHDDS subunit, recently discovered by our collaborator Dr. Serena Galosi at Sapienza University of Rome. The mutations include: G35E, R37C, P233R, I135T, R205Q and S213N.These heterozygous mutations were identified by exome-sequencing of 20 patients suffering from various neurological abnormalities such as: developmental delay; generalized tremor; epilepsy; myoclonic seizures; ataxia; mild to severe intellectual disability; parkinsonism; hallucinations and anxiety. Mapping these mutations on the structure revealed that the majority cluster around the active site of NgBR/DHDDS complex and are involved in substrate binding (SI appendix, Fig. S14A). The β-phosphate group of FPP substrate is hydrogen-bonded to the backbone amide of Gly35, which is localized on the P-loop, well established to be involved in FPP binding. Therefore, replacing Gly with Glu would result in steric clashes with nearby residues and hence perturb packing of the P-loop and might even disrupt the conformation of Arg38 on the proceeding α1 helix, which is also involved in FPP binding. In addition, the side chain of Arg37 is stabilized by a network of salt bridges with the β-phosphate group of FPP, Glu89 on DHDDS and the main chain carboxylate group of Lys293 on the C-terminus of NgBR. Therefore, introducing an uncharged residue like cysteine at this

position could abolish the salt bridges with the β-phosphate group of FPP as well as the C-terminus of NgBR (SI appendix, Fig. S14B). Similarly, the side chain of Arg205 forms salt bridges with the pyrophosphate group of IPP and replacement of Arg residue with Gln would eliminate these binding interactions (SI appendix, Fig. S14C). Although replacing Ser with Asn at position 213 can still maintain hydrogen bonding with the β-phosphate group of IPP, introducing a bulky side chain at this region would result in steric clashes with nearby residues, hence leading to a structural destabilization. While all residues mentioned above are directly involved in substrate binding, Pro233 and I135 are exception to this pattern. Pro233 is localized within a loop that connects βF with α7 and is involved in hydrophobic packing against Tyr39 on α1, which is involved in FPP binding (SI appendix, Fig. S14D). Therefore, replacing Pro with a charged residue like Arg would disrupt packing of α1 helix and hence binding to FPP substrate. I135 on the other hand is localized within α4 helix distal to the active site and it is unclear how a mutation at this position might interfere with *cis*-PTase enzymatic activity.

2.3.5 NgBR mutations and Parkinson's disease

A recent exome-sequencing study by Guo, et.al (70) has identified number of mutations on the *NUS1* gene that were shown to contribute to the etiology of Parkinson's disease. Most of the reported mutations (11 out of 15) occur within *cis*-PTase core domain of NgBR which is well resolved in our current structure (Fig 2.4A). Intriguingly, mapping these mutations onto the structure clearly revealed a scattered pattern that does not seem to affect dimerization or substrate binding. Next, I sought to measure the solvent accessible surface area of individual mutation residues to see if any pattern could emerge that may account for their pathogenicity. Again, no underlying pattern was observed as most residues (7 out of 11) were exposed to solvent (Fig 2.4D). Therefore, it is still unclear whether these mutations affect *cis*-PTase activity in vivo, or impact some other mechanism involving NgBR that is not related to dolichol synthesis.

A more careful examination of the structural role played by PD mutations revealed that G91C could indirectly affect *cis*-PTase activity through the C-terminal -RXG- motif. Notably, Gly-91 is located on the NgBR N-terminal helix (α1) (highlighted in green, Fig 2.4A) and is close to lys-96, present at the end of the helix. The lys residue in turn, is involved in a network of hydrogen bonding with the backbone carbonyl of Tyr-284 and the side chain of Gln-289, thus stabilizing the -RXG- motif (Fig 2.4B). Given the critical position of Gly-91 in mediating contacts between helix α1 and the rest of the protein, replacement with Cys can be disruptive to the structure since it will interfere with the helical packing as well as interactions with the C-terminal -RXG- motif through Lys-96. To further investigate the proposed role of Gly-91, I expressed and purified $NgBR^{G91C}$/DHDDS mutant using the same expression/purification system employed for crystalizing studies . Next, I measured the steady-state activity of the WT and the

mutant in the presence of phosphatidylinositol. In agreement with its predicted role, G91C exhibited ~ 40% reduction in enzymatic activity compared to the WT enzyme (Fig 2.4C). These data are in line with previous observation that a splice variant of NgBR reducing its mRNA levels by 50% also increases PD risk (70). Furthermore, the loss of *NUS1* gene in *Drosophila* reduced it climbing ability, dopamine levels, and number of dopaminergic neurons (70). Interestingly, dolichol accounts for ~ 14% of the dry weight of neuromelanin, a dark pigment presents at high concentration in dopaminergic neurons of the human substantia nigra (SN) (91, 92), and a massive degeneration of the SN is considered one of the hallmarks of Parkinson's disease. Nevertheless, further studies are needed to determine whether low dolichol levels can impact the normal glycosylation of certain proteins or may affect other functions that is independent of protein glycosylation. In summary, our structural and biochemical studies provide a novel insight into the role of dolichol biosynthesis in neurodegenerative diseases.

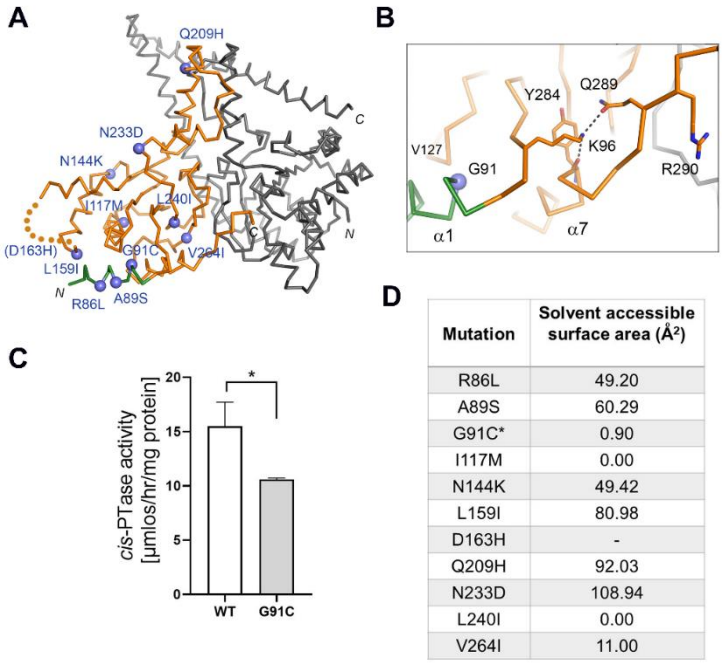

D

Mutation	Solvent accessible surface area (Å²)
R86L	49.20
A89S	60.29
G91C*	0.90
I117M	0.00
N144K	49.42
L159I	80.98
D163H	-
Q209H	92.03
N233D	108.94
L240I	0.00
V264I	11.00

Figure 2.4 Missense NgBR mutations associated with Parkinson's disease.

(A) NgBR mutations related to Parkinson's disease are shown as purple spheres and labeled. DHDDS is colored in gray and NgBR is colored in orange except for the N-terminal helix (α1) which is shown in green.
(B) Detailed view showing the location of G91C disease mutant within NgBR colored orange except for α1 helix, shown in green. Gly-91 is involved in hydrophobic packing against Val-127. Lys-96 forms hydrogen bonds with Tyr-248 and Gln-289, which stabilize the C-terminal -RXG- motif.
(C) *cis*-PTase activity was measured using purified wildtype and NgBR disease mutant, G91C. The mutant exhibits ~ 40% reduction in *cis*-PTase activity compared to
wildtype enzyme. The values are the mean ±S.D. of three independent measurements.
(D) The majority of the mutated residues is solvent-exposed. The solvent accessible surface area ($Å^2$) was calculated using GETAREA server.

2.3.6 Regulation of *cis*-PTase activity by membrane binding

Unlike the soluble UPPS enzymes, heteromeric *cis*-PTases are commonly found to be associated with a hydrophobic platform such as membrane bilayers, lipid droplets and rubber particles (46, 93, 94). The very N-terminus of NgBR (residues 1-56, not included in the structure) harbors two hydrophobic segments predicted to bind to the ER membrane. In addition, our refined structure revealed a unique N-terminal segment within the DHDDS subunit that is absent in the bacterial UPPS enzymes. The N-terminal region consists of a random coil (residues 1-10) and a short α-helix (α_0; residues 11-21). Intriguingly, the coil exhibits a unique conformation whereby its bulky Trp (W3) extends into the hydrophobic tunnel between the two helices, α2 and α3 (Fig 2.5A, left panel; Fig 2.5B); such conformation would be inadequate for product chain elongation during catalysis. Therefore, we hypothesize that a conformational change displacing the coil from the hydrophobic tunnel is essential for proper chain elongation (Fig 2.5A, right panel). A more detailed analysis of the short α0 helix revealed the presence of three hydrophobic residues (Trp-12,Phe-15, Ile-19) that are exposed to solvent. Furthermore, a sequence alignment analysis confirmed the conservation of this hydrophobic patch among DHDDS orthologs, suggesting a possible conserved role for α0 helix in membrane binding (Fig 2.5C). In order to determine the functional consequences of such hydrophobic conservation, I expressed and purified a triple DHDDS mutant, whereby all three hydrophobic residues were substituted with Ala (W12A/F15A/I19A). The mutant displayed similar basal activity as the WT enzyme in the absence of phosphatidylinositol. However, the mutant was no longer potently stimulated with phosphatidylinositol (Fig 2.5D). Moreover, a TLC analysis of the reaction product revealed a difference in the length of the polyprenol formed by the triple mutant compared to WT enzyme. Instead of the dominant 19 isoprene units seen with the WT enzyme,

polyprenols as long as 22 isoprene units were formed as the dominant product by the triple mutant (Fig 2.5E). Taken together, we hypothesize that in addition to NgBR, DHDDS plays an essential role in membrane binding and activation through its N-terminal α0-helix, which acts as a membrane sensor. The binding is transient but sufficient to trigger a conformational change characterized by the displacement of the N-terminal coil; thereby unblocking the hydrophobic tunnel and destabilizing the enzyme: product complex to facilitates product release (see below).

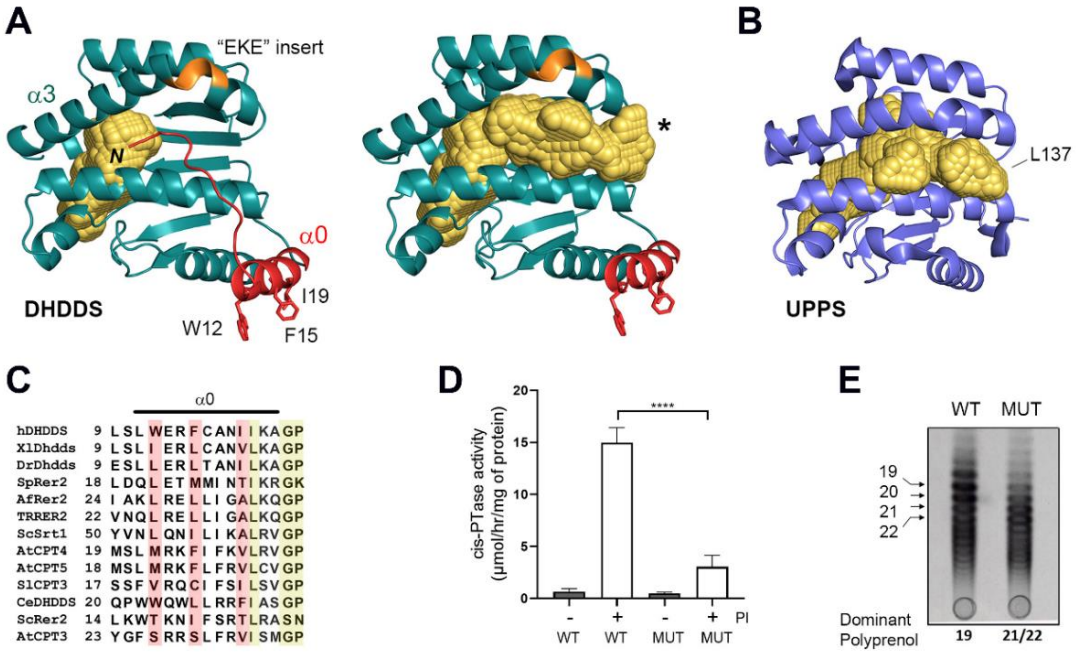

Figure 2.5 DHDDS's helix α0 functions as a membrane sensor.

(A) A cartoon representation of DHDDS subunit colored in deep teal. The hydrophobic cavities of DHDDS before (left) and after (right) N-terminal loop deletion (residues 1-10) are shown in yellow. The N-terminal loop and α0 helix are shown in red; the side chains of the three exposed hydrophobic residues are shown and labeled. The hydrophobic cavity was generated using the 3V web server (95).

(B) A cartoon representation of *E.coli* UPPs (PDB entry 1X06) monomer colored in purple. The hydrophobic cavity is shown in yellow. Leu-137 involved in chain length control in UPPS is located at the end of the cavity.

(C) Sequence alignment showing the conservation of three hydrophobic amino acids at the N-terminal helix α0 among DHDDS orthologs (highlighted in red). Conserved residues are highlighted in yellow. Proteins represented in this alignment are orthologs of human DHDDS *cis*-PTase subunit as follows: hDHDDS (human, UniProtKB Q86SQ9-1), XlDhdds (*Xenopus laevis;* UniProtKB Q7ZYJ5), DrDhdds (*Danio rerio*, UniProtKB Q6NXA2*)*, CeDHDDS (*Caenorhabditis elegans*, UniProtKB Q5FC21*)*, ScRer2 (*Saccharomyces cerevisiae*, UniProtKB P35196), ScSrt1 (*Saccharomyces cerevisiae*, UniProtKB Q03175), SpRer2 (*Schizosaccharomyces pombe*, UniProtKB O14171), TrRER2 (*Trichoderma reesei*, *UniProtKB - G0ZKV6), AfRer2 (Aspergillus fumigatus UniProtKB - Q4WQ28),* SlCPT3 (*Solanum lycopersicum*, UniProtKB K7WCI9), AtCPT3 (*Arabidopsis thaliana*, UniProtKB Q8S2T1), AtCPT4 (*Arabidopsis thaliana*, UniProtKB Q8LAR7), AtCPT5 (*Arabidopsis thaliana*, UniProtKB Q8LED0)

(D) Phospholipid stimulation of wildtype and W12A/F15A/I19A triple mutant is shown. Stimulation was compared by measuring *cis*-PTase activity of purified wildtype and DHDDS triple mutant in the presence and absence of 1% phosphatidylinositol (PI). The values are the mean ±S.D. of five to eight independent measurements.
(E) Reverse phase TLC separation of dephosphorylated products from *cis*-PTase activity of WT and DHDDS triple mutation (W12A/F15A/I19A) denoted as MUT. Numbers correspond to the dominant polyprenols in each sample are shown at the bottom of the plate. The position of the polyprenol standards is shown on the left.

2.3.7 The mechanism of product chain elongation

While homodimeric *cis*-PTases generate a product with distinct chain length, heteromeric enzymes have the incredible ability of generating longer chain polyprenols characterized by a distribution pattern. As shown in Fig 2.5E, the human NgBR/DHDDS complex synthesizes C_{95} polyprenol as the dominant product, along with varying amounts of other polyprenols that differ by one isoprene unit. The current model of product chain elongation by *cis*-PTases is based on number of structural and biochemical studies performed on homodimeric UPPS enzymes (6, 50, 96, 97). According to these studies, the volume of the hydrophobic tunnel correlates well with the size of the synthesized product. However, our structural analysis of the NgBR/DHDDS complex suggests that this might not be the case for heteromeric enzymes. After manually removing the N-terminal coil which occludes the hydrophobic tunnel (Fig 2.5A), I used 3V server (95) to calculate the volume of the tunnel which turned out to be around 1,300 $Å^3$. This volume is similar to that of *E.coli* UPPS (1,200 $Å^3$) which synthesizes medium chain C_{55} products (Fig 2.5B). Therefore, to accommodate longer-chain products, two scenarios are possible: the first involves a conformational change that would greatly expand the hydrophobic tunnel, and the second involves pushing the polyprenol chain out of the tunnel. In an attempt to rationalize the first model, we carefully examined the structure of the human complex to look for obvious differences that would allow for the synthesis of longer-chain products. Intriguingly, we were able to identify a stretch of 3 amino acids (Glu-107, lys-108, Glu-109) located at the middle of α3-helix of DHDDS. Multiple sequence alignment of other eukaryotic *cis*-PTases revealed the presence of a similar insertion on DHDDS orthologs, consisting of three to five amino acids (Fig 2.6A). Although the presence of three extra residues creates a kink or a bulge in the α3 helix of DHDDS, based on our computational measurements, the insert does not seem to influence the

volume of the hydrophobic tunnel (Fig 2.5A; left panel and Fig 2.6C). To test whether the insert may contribute to the synthesis of longer-chain products, a construct harboring ΔEKE deletion on the DHDDS subunit was generated and transformed into the yeast triple deletion strain (*rer2*Δ, *srt1*Δ, *nus1*Δ) along with WT NgBR. HPLC analysis of the total lipids isolated from yeast cells revealed that the ΔEKE deletion strain synthesized shorter products (dominant: Dol-17 (C_{85})) compared to Dol-20 (C_{100}) generated by the WT enzyme (Fig 2.6B). Theoretically, deleting the insert within DHDDS would make the tunnel similar to that of UPPS enzymes. Nevertheless, the length of polyprenols generated by the mutant remained > C_{55}. Furthermore, a product distribution pattern can still be observed. Taken together, these data suggest that the EKE insert at the α3 helix might not necessarily account for the longer chain product phenomena observed in heteromeric enzymes. Therefore, further structural studies involving a co-crystal with the reaction product are needed to better understand conformational changes taking place during chain elongation. Interestingly, a previous crystal structure of *E.coli* UPPS in complex with Triton X-100, a molecule that may mimic the reaction product, revealed a conformational change involving an upward movement of the α3-helix became less kinked compared to the substrate-bounded form (52). Although this conformation has the potential to increase the size of the hydrophobic tunnel, the protein is unlikely to be in this state during product chain elongation process. This is true since a large movement of the α3-helix will misplace its N-terminal region, which is involved in binding the pyrophosphate moiety of the allylic substrate, hence interfering with subsequent elongation steps. Accordingly, the second model where part of the polyprenol chain exits the hydrophobic tunnel seems more plausible. In a previous mutagenesis experiment on the *E.coli* UPPS, Ko et al. (98) reported that replacement of L137, located at the bottom of the tunnel with Ala resulted in the formation of a range of products with C_{75} as the major product in

the absence of a detergent (Fig 2.5B). These data suggest that L137, equivalent to C148 in DHDDS, functions as the floor of the tunnel that could block further product elongation.

A schematic diagram illustrating the second plausible model for the chain elongation process within the hydrophobic tunnel of DHDDS is shown in Fig 2.6D. According to this model, the polyprenol chain will continue to grow inside the tunnel until reaching ~ C_{65} or 13 isoprene units (tunnel volume ~1300 $Å^3$; each isoprene unit occupies ~ 100 $Å^3$), after which the product exits the tunnel and becomes exposed to solvent, where it can grow indefinitely. Such model is in contrast with short and medium-chain homodimeric *cis*-PTase enzymes, in which the chain-elongation process is solely taking place inside the tunnel, hence is restricted by the size of the tunnel. If the product continues to grow beyond the walls of the tunnel, then it might be reasonable to assume that the stability of the enzyme: product complex will have a great impact on product size. Therefore, any interaction between the exposed portion of the hydrophobic polyprenol and its surrounding environment, including a detergent micelle, a membrane bilayer or a lipid droplet can be energetically unfavorable and will disrupt the enzyme: product complex, leading to product release. Indeed, previous studies on *E.coli* UPPS showed that L137A mutant failed to produce long-chain products in the presence of Triton X-100 (98). Similarly, purified NgBR/DHDDS complex tends to form shorter chain polyprenols in the presence of phospholipids and vice versa. Regarding the role of EKE insert within α3 helix, we hypothesize that it may stabilize the enzyme: product complex, perhaps by allowing a greater conformational flexibility to α3 helix and its surrounding region. In summary, our proposed model provides a plausible explanation for the synthesis of long-chain products. Additionally, the model attributes the changes in the environment surrounding the enzyme: product complex to the observed product distribution pattern that is unique to heteromeric *cis*-PTase enzymes.

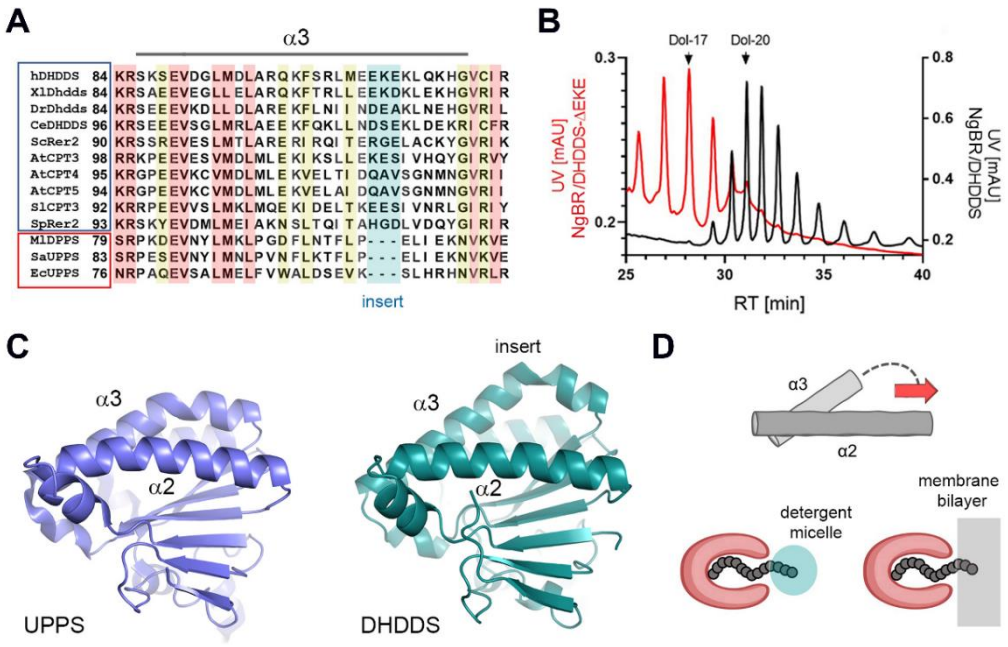

Figure 2.6 Mechanism of chain elongation by heteromeric *cis*-PTases

(A) Multiple amino acid sequence alignment comparing α3 helix between DHDDS orthologs and homodimeric *cis*-PTases. Highly conserved residues are highlighted in red and less conserved ones are shown in yellow. Region corresponding to DHDDS EKE insert is highlighted in blue; the region is missing in homodimeric enzymes and a gap is present instead. Proteins represented in this alignment are: single subunit *cis*-PTs: EcUPPS (*Escherichia coli*, UniProtKB P60472), MlDPPS (*Micrococcus luteus*, UniProtKB O82827), SaUPPS (*Sulfolobus acidocaldarius*, UniProtKB Q9HH76). Orthologues of human DHDDS *cis*-PTase subunit: hDHDDS (human, UniProtKB Q86SQ9-1), XlDhdds (*Xenopus laevis*, UniProtKB Q7ZYJ5), DrDhdds (*Danio rerio*, UniProtKB Q6NXA2), CeDHDDS (Caenorhabditis elegans, UniProtKB Q5FC21), ScRer2 (*Saccharomyces cerevisiae*, UniProtKB P35196), SpRer2 (*Schizosaccharomyces pombe*, UniProtKB O14171), SlCPT3 (*Solanum lycopersicum*, UniProtKB K7WCI9), AtCPT3 (*Arabidopsis thaliana*, UniProtKB Q8S2T1), AtCPT4 (*Arabidopsis thaliana*, UniProtKB Q8LAR7), AtCPT5 (*Arabidopsis thaliana*, UniProtKB Q8LED0)
(B) HPLC analysis of chain length of dolichol generated by WT and ΔEKE DHDDS mutant in yeast cells. The dolichol peaks were identified and labeled on top of the chromatogram. The WT cells yielded the main compound Dol-20 compared to Dol-17 in ΔEKE mutant. The chain length and identity of lipids were confirmed by comparison with external standards of a polyprenol (Pren-10 – Pren-24) and dolichol (Dol-17 – Dol-23) mixtures.
(C) Structural comparison between *E. coli* UPPS (PDB ID 1X06) monomer and human DHDDS subunit. The EKE insert within α3 helix of DHDDS creates a bigger bulge that may contribute to the stabilization of the enzyme:product complex during chain elongation.

(D) Schematic diagram illustrating the proposed chain elongation mechanism for *cis*-PTases. Red arrow indicates the direction of product elongation. Exposed hydrophobic isoprene units may increasingly destabilize the enzyme:product complex by interacting with detergent micells (blue) or lipid bilayers (grey).

2.4 Discussion and Future Direction

Here, I show the first crystal structure of NgBR/DHDDS complex solved at 2.3 Å, which provides novel insights into the molecular mechanism of heteromeric *cis*-PTase enzymes. The structure reveals the heteromeric assembly of NgBR and DHDDS, mainly through a canonical *cis*-PTase interface region but also partially by a newly identified C-terminal region on the DHDDS subunit. In addition, the structure confirms NgBR role in the overall catalytic mechanism through its C-terminal -RXG- motif, which completes the active side to participate in catalysis and substrate binding. Furthermore, the newly identified N-terminal domain on DHDDS plays a key role in enzyme activation by membrane binding. Our studies also provide a plausible mechanism for product chain elongation by heteromeric enzymes that rationalize the length and distribution of the synthesized polyprenols. Finally, the structure provides a detailed analysis of various loss-of-function mutations associated with human diseases. Collectively, these results advance our current understanding of the dolichol biosynthesis pathway necessary for protein glycosylation.

Shortly after the publication of our structural work presented herein, another research group independently demonstrated the successful crystallization of the human NgBR/DHDDS enzyme in complex with FPP and Mg^{2+} ion (99). The study revealed similar heteromeric assembly of the two subunits and further confirmed the unique architecture of DHDDS's N-, and C-terminal regions observed in our structure. Additionally, similar to our findings, NgBR C-terminal -RXG- motif traversed the dimeric interface to complete the active side of the DHDDS subunit and participate in substrate binding.

The overall structural fold of the heteromeric NgBR/DHDDS complex resembles that of all known homodimeric *cis*-PTases, whereby each subunit consists of a β-sheet core surrounded

by α helices. Moreover, the heteromeric complex seems to maintain the canonical interface region commonly found in homomeric enzymes. To further support the heteromeric assembly of the two subunits, DHDDS evolved a unique C-terminal region, which adopts a "helix-turn-helix" organization. Sequence alignment analysis of multiple DHDDS orthologs revealed a poor conservation of their C-terminus domain. Therefore, the functional role of DHDDS's C-terminus can only be deduced via structural studies. Our refined structure demonstrates the C-terminal helices of DHDDS to form multiple binding interactions with NgBR and within DHDDS, thus creating an additional interface that provides extra support for the heteromeric complex. This notion was further confirmed by our yeast complementation data, which clearly show the essential role of this region in maintaining the integrity of the protein complex.

The structural similarity between the active site of NgBR/DHDDS complex and homodimeric *cis*-PTases suggest a conserved catalytic mechanism among this family of enzymes. The pyrophosphate group of the allylic and homoallylic substrates is stabilized by a network of interactions with several polar residues located at the entry of S1 and S2 sites, respectively. The prenyl tail of the substrates extends into a tunnel lined with multiple hydrophobic residues to bind and stabilize the allylic substrate and reaction intermediate during catalysis. A Mg^{2+} ion is coordinated by the catalytically conserved Asp-34, the pyrophosphate moiety of both substrates and three water molecules. In addition to these shared features, our data presented here provide the first structural evidence for the involvement of NgBR in the overall catalytic mechanism through its C-terminal -RXG- motif. Consistent with this notion, mutations on the C-terminal -RXG- motif were previously shown to reduce the catalytic activity and IPP binding (9). Therefore, despite the low sequence similarity with *cis*-PTase, NgBR remarkably maintains a key structural feature shared with homodimeric enzymes, which serves

the same function. In addition, our current structure further corrects previous assumptions which limited the role of NgBR to stabilization of the heteromeric complex.

Based on structural comparisons with short and medium-chain *cis*-PTases, long-chain, heteromeric *cis*-PTase enzymes were predicted to exhibit a large hydrophobic tunnel to accommodate the long-chain product. However, our refined structure and computational measurements clearly suggest that this might not be the case due to the similarity in the tunnel volume of DHDDS and that of medium-chain *E.coli* UPPS (1,300 for DHDDS vs. 1,200 for *E.coli* UPPS). Furthermore, deletion of the EKE insert at the α3 helix on DHDDS still produced a polyprenol that is > C_{55} as the dominant product along with additional polyprenols that differed by one isoprene unit, thus retaining the two key product features that are unique to heteromeric enzymes. Given these observations, we propose a plausible model for the mechanism of chain elongation by the long-chain NgBR/DHDDS protein complex (SI appendix, Fig.S15). The process starts with the binding of an allylic substrate (i.e. FPP) to the S1 site, followed by IPP-Mg^{2+} complex at the S2 site. A transient membrane binding facilitated by the N-terminal α0 of DHDDS results in a conformational change that would displace the N-terminal coil from the hydrophobic tunnel to allow for the chain elongation process. Following several rounds of IPP condensations (~ 13 isoprene units), the hydrophobic tail of the product is pushed out of the tunnel thereby allowing the incorporation of additional isoprene units. The EKE insert at the α3 helix may provide the appropriate flexibility as the product extends outside the tunnel. The resulting enzyme: product complex is destabilized by membrane binding, consequently leading to product release. To facilitate this process, the enzyme may undergo another conformational change through the α3 helix on DHDDS, which becomes less kinked to increase the size of the tunnel. Clearly, the model proposed herein suggests that subtle environmental changes can affect

the stability of the enzyme: product complex, leading to the observed product distribution in heteromeric enzymes. In the case of extensively long *cis*-PTases such as rubber synthase, additional players might provide incredible stability for the enzyme in its product-bounded form. This notion was previously supported by earlier studies on rubber synthase, demonstrating the requirement of other components including a rubber particle, a rubber elongation factor (REF), and several small stabilizing proteins (SRPP) (56).

Given the essential role of protein glycosylation for various cellular functions, mutations on both NgBR and DHDDS subunits have been associated with serious human diseases. Determining the crystal structure of the complex allowed us to map and structurally analyze these mutations, many of which clustered around the active site region. An exception is the Parkinson's disease mutations as most of them scatter throughout NgBR structure and do not seem to influence protein folding or dimerization. Therefore, the molecular mechanism underlying their etiology remains unclear. However, one Parkinson's mutation, G91C, is located within the N-terminal helix of NgBR and seems to indirectly influence *cis*-PTase activity by disrupting the C-terminal -RXG- motif involved in catalysis and substrate binding. In addition, our structure provides the first insight into the molecular mechanism of K42E, the most commonly occurring mutation among Ashkenazi Jewish patients diagnosed with the autosomal recessive retinitis pigmentosa. We show that a mutation at this position disrupts a conserved salt bridge formed with Glu-233 and could perturb DHDDS's α1 helix involved in FPP binding, consistent with our previous functional studies on the purified mutant (9). It is important to note that in most cases, the disease severity in patients harboring *cis*-PTase mutations correlates well with their genotype and their measured enzymatic activity. For instance, the homozygous R290H mutation associated with the severe, multi-systemic CDG type I, displayed only ~20% *cis*-PTase

activity when measured from patients' fibroblasts as well as the purified mutant (9, 39). In contrast, heterozygous mutations associated with the less severe developmental and epileptic encephalopathy (DEE) displayed up to 60% activity in fibroblasts with purified mutants being up to ~10% active. An exception is the K42E mutation which results in a marked reduction in *cis*-PTase activity (enzyme was ~15% active), yet patients with this homozygous mutation displayed a non-syndromic retinitis pigmentosa with no obvious defects in other tissues and organs. A recent genetic model of mice with a global knock-in of the homozygous K42E mutation showed a marked gliosis with no evidence of retinal degeneration or defective protein N-glycosylation in retinal tissues (100). Furthermore, selective ablation of *DHHD* in retinal tissues of mice showed a profound and rapid retinal degradation, again with no effect on protein N-glycosylation (101, 102). In another genetic study using zebrafish as a model, it was shown that a global knockdown of *DHDDS* resulted in the loss of photoreceptor outer segment and visual function (103). Collectively, these studies suggest that the pathology of retinitis pigmentosa might not be mediated by a defective protein glycosylation process and that it may involve other unknow functions of dolichols. As mentioned earlier, patients harboring the homozygous R290H also develop retinitis pigmentosa. Intriguingly, in both K42E and R290H patients, an aberrant dolichol ratio was observed whereby Dol-18 became the dominant polyprenol instead of Dol-19 (39, 66). It is possible that toxic accumulation of these aberrant dolichols might cause a retinal damage. However, there is no current evidence demonstrating the precise effect of aberrant dolichol chain length on cellular functions.

Clearly, the structural work presented in this dissertation is the first attempt in the field to gain an insight into molecular mechanism of heteromeric *cis*-PTases. The structure reveals many novel aspects regarding the heteromeric assembly of the two subunits and proposes a rational

model for the mechanism of chain elongation. Moreover, our structural-functional analysis of NgBR/DHDDS disease mutations provides a framework to better understand the molecular mechanism underlying their pathogenicity and might aid in the development of new therapeutic strategies that could delay the progression of some clinical symptoms associated with these mutations. Future work might involve a structural characterization of NgBR N-terminal region harboring the predicted membrane-binding domains to better understand its membrane topology. Previous work demonstrated the presence of a signal anchor consisting of the first 23 amino acids at the N-terminus of NgBR (45). Therefore, this region might serve as an important component in the selection mechanism for ER localization. To gain an insight into the structure of the N-terminus, one strategy might involve a reconstitution of the full length NgBR/DHDDS complex into nanodiscs with appropriate size and lipid composition, followed by a structural analysis using cryo-EM technique. Another important structural feature that demands further investigation is the newly identified N-terminal region of DHDDS. Results presented in this work suggest a possible conformational change induced by phospholipid binding; such a conformational change involves the displacement of the N-terminal coil containing a bulky Trp-3. To further test this model, future studies might involve fluorescence binding experiment to monitor changes in fluorescence of Trp-3 upon adding phospholipids. An alternative approach might involve a hydrogen-deuterium exchange mass spectroscopy (HDX-MS) analysis in the presence and absence of phospholipids.

In addition, our knowledge regarding regulation of *cis*-PTase activity is still limited despite its crucial role in protein glycosylation. Interestingly, recent studies revealed that some homodimeric *cis*-PTase enzymes can utilize dimethyl allyl pyrophosphate (DMAPP) as the homoallylic substrate to catalyze a head-to-middle condensation reaction, leading to the

formation of branched isoprenoids. Our preliminary data on the purified human complex showed that although the enzyme failed to use DMAPP as the homoallylic substrate to catalyze the reaction, a slight enhancement in *cis*-PTase activity was observed upon adding DMAPP at low concentrations in the presence of enzyme's substrates. Recent work by Zhao et.al (77) suggested a possible binding site for a farnesylated Ras at the NgBR subunit. Accordingly, we hypothesize that this region might serve as an allosteric binding site for the regulation of enzymatic activity by small molecules. Therefore, one possible follow-up experiment might involve solving the crystal structure of NgBR/DHDDS in complex with DMAPP to better understand its role in enzyme activation. Besides allosteric activation, inhibiting *cis*-PTase activity could be another interesting field to explore due to the decent amount of work showing an altered NgBR expression in cancerous tissue, which might result in changes in *cis*-PTase activity. Moreover, the bacterial UPPS has been a common target for the development of new and effective antibacterial drugs. Nevertheless, one important issue that may halt the development of many of these drugs is their specificity in targeting the bacterial rather than the human enzyme. Therefore, with our newly solved structure, it might be possible to virtually screen thousands of compounds against the human enzyme which will narrow down the number of molecules with inhibitory effect and could potentially accelerate the development of hit molecules. In summary, the structural work presented in this dissertation is the first attempt in the field to decipher the molecular mechanism of a heteromeric *cis*-PTase enzyme and serves as a framework for future studies on the dolichol biosynthetic pathway.

SI APPENDIX

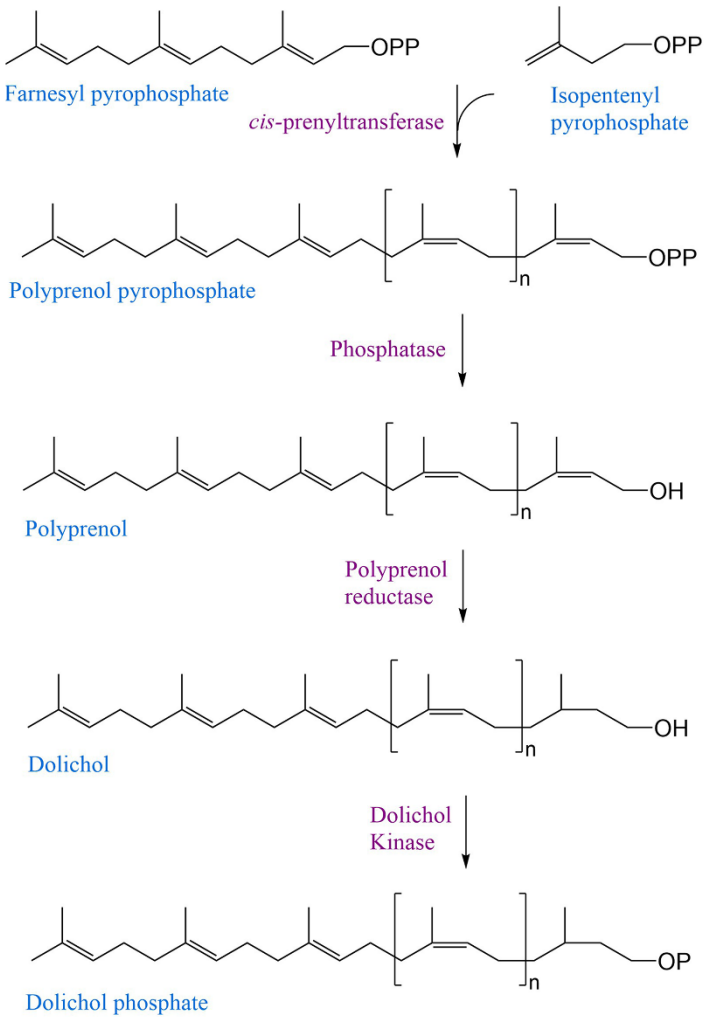

Figure S1. De novo synthesis of dolichol from FPP and IPP.

Cis-PTase catalyzes the condensation of farnesyl pyrophosphate with multiple isopentenyl pyrophosphate molecules, resulting in the formation of polyprenol pyrophosphate. The condensation is followed by dephosphorylation and reduction to form dolichol, which is further phosphorylated by a dolichol kinase to yield dolichol phosphate, the main sugar carrier lipid during protein glycosylation.

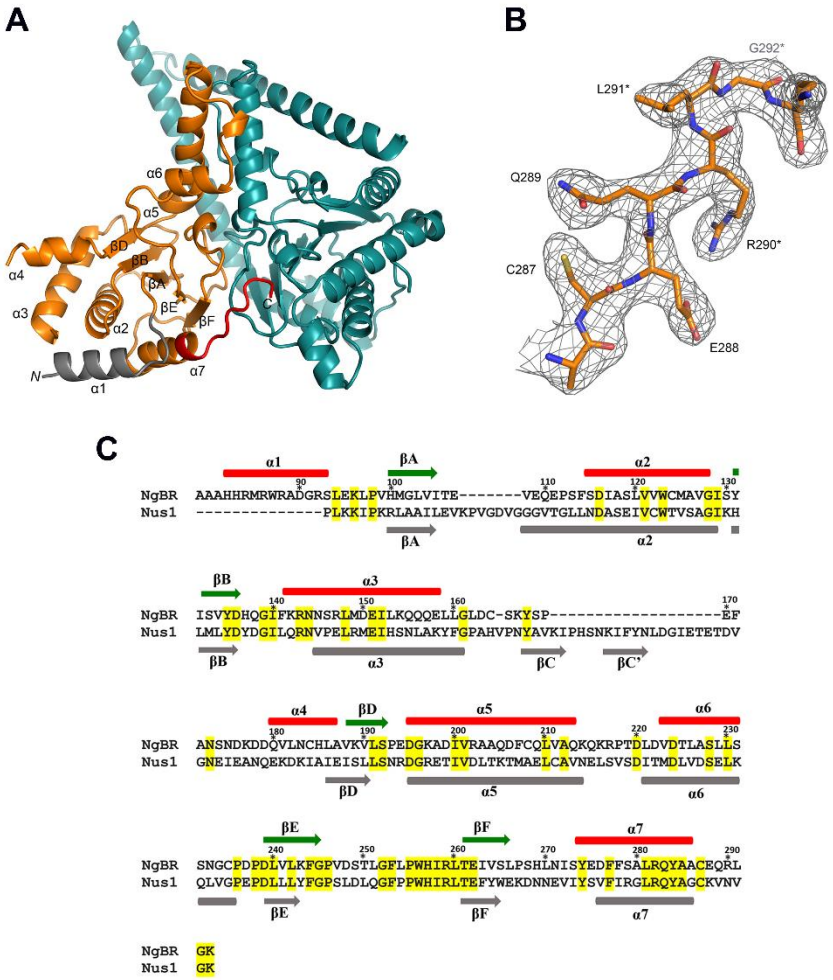

Figure S2. Structural details of the NgBR subunit.

(A) Ribbon diagram of NgBR/DHDDS complex; NgBR colored in orange and DHDDS in deep teal. The N-terminal helix of NgBR is colored in gray and the C-terminal loop in red. Secondary structure elements as well as N- and C-termini of NgBR are labeled on the structure.
(B) 2Fo-Fc electron density map of the C-terminal -RXG- motif of NgBR contoured at 1.0 σ. The motif residues are indicated by the asterisks.
(C) Partial amino acid sequence of NgBR subunit (residues 79-293) is aligned with partial sequence of yeast NUS1 subunit (residues 148-375). Numbers and secondary structure elements shown above the sequence correspond to that of NgBR. NUS1 secondary structure elements are shown in gray, below the sequence. Conserved residues are highlighted in yellow.

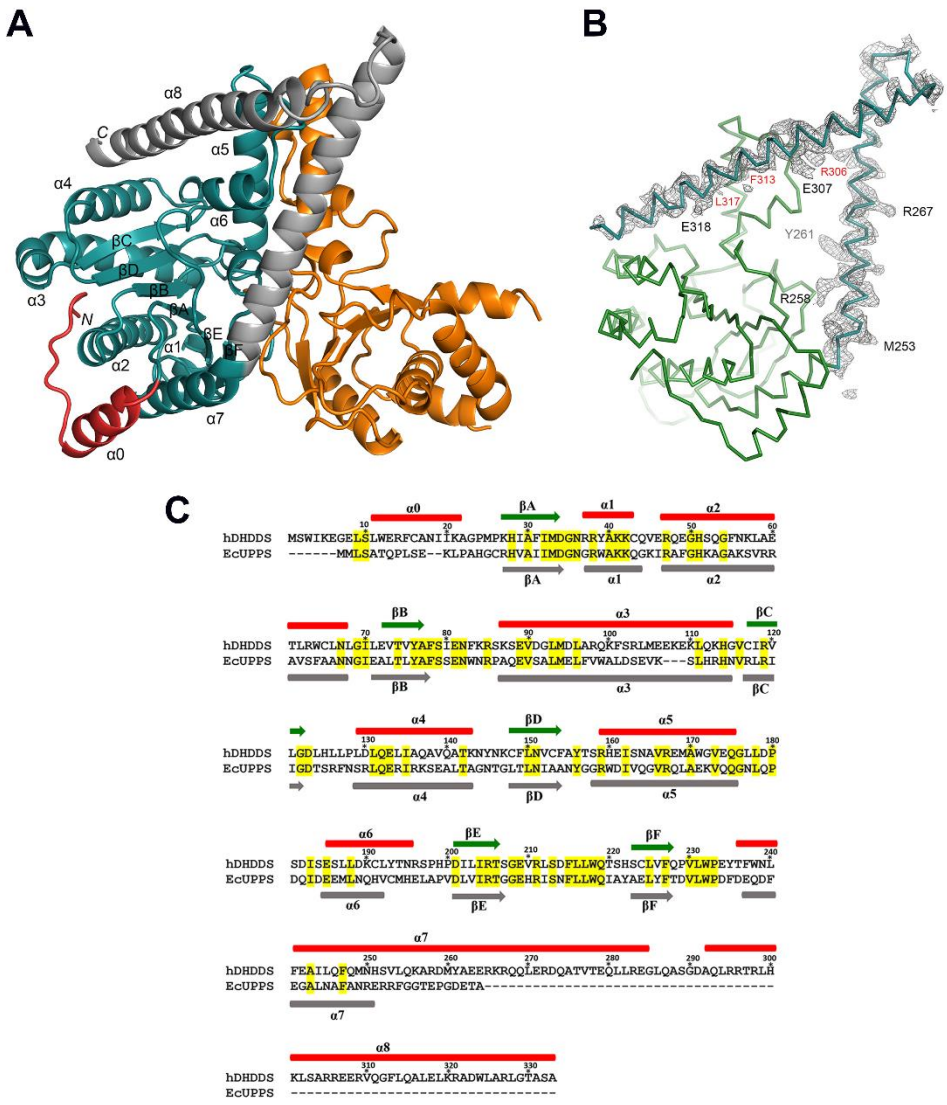

Figure S3. Structural details of the DHDDS subunit.

(A) Ribbon diagram of NgBR/DHDDS complex; NgBR colored in orange, DHDDS in deep teal. The N-terminal region of DHDDS is colored red and the C-terminal helices are in gray. Secondary structure elements as well as N- and C-termini of NgBR are labeled on the structure.
(B) 2Fo-Fc electron density map of the C-terminal helices of DHDDS contoured at 1.0 σ. Residues mutated in the yeast complementation experiment are labeled in red.
(C) The full-length amino acid sequence of DHDDS subunit (residues 1-333) is aligned with full length *E.coli* UPPS (residues 1-253). Numbers and secondary structure elements shown above the sequence correspond to that of DHDDS. *E.coli* UPPS secondary structure elements are shown in gray, below the sequence. Conserved residues are highlighted in yellow.

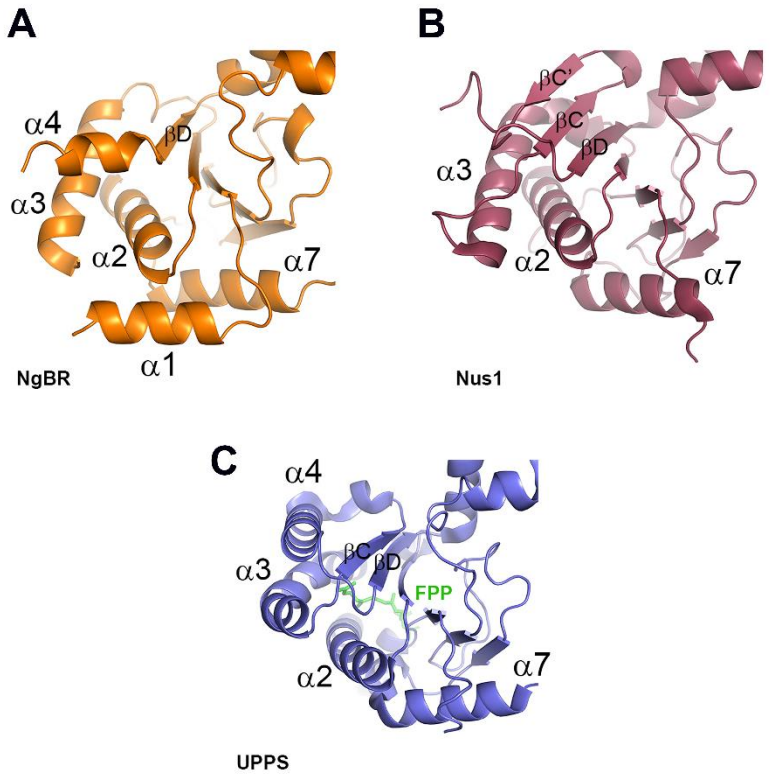

Figure S4. Structural comparison of NgBR, Nus1 and UPPS.

A ribbon diagram comparing the structure of (A) NgBR (orange) to that of (B) yeast Nus1 (Ruby, PDB ID 6JCN) and (C) UPPS (Purple, PDB ID 4H8E). NgBR possesses α4 helix, which differs from that of UPPS and is replaced by βC and βC' in Nus1. An additional α1 helix is present in NgBR N-terminal region and is not observed in Nus1.

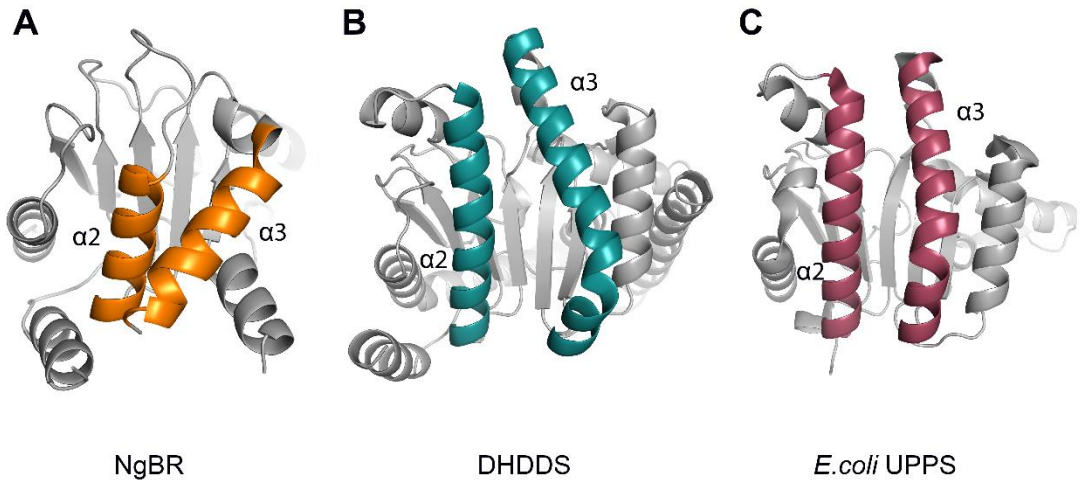

Figure S5. Active site comparison of NgBR, DHDDS and UPPS.

A ribbon diagram highlighting the hydrophobic cavity of NgBR (orange), DHDDS (cyan) and UPPS (pink). NgBR exhibits a short α3 helix, which directly associates with α2 helix, leading to the collapse of the active site cavity. Such architecture may account for the inability of NgBR to catalyze the chain elongation process.

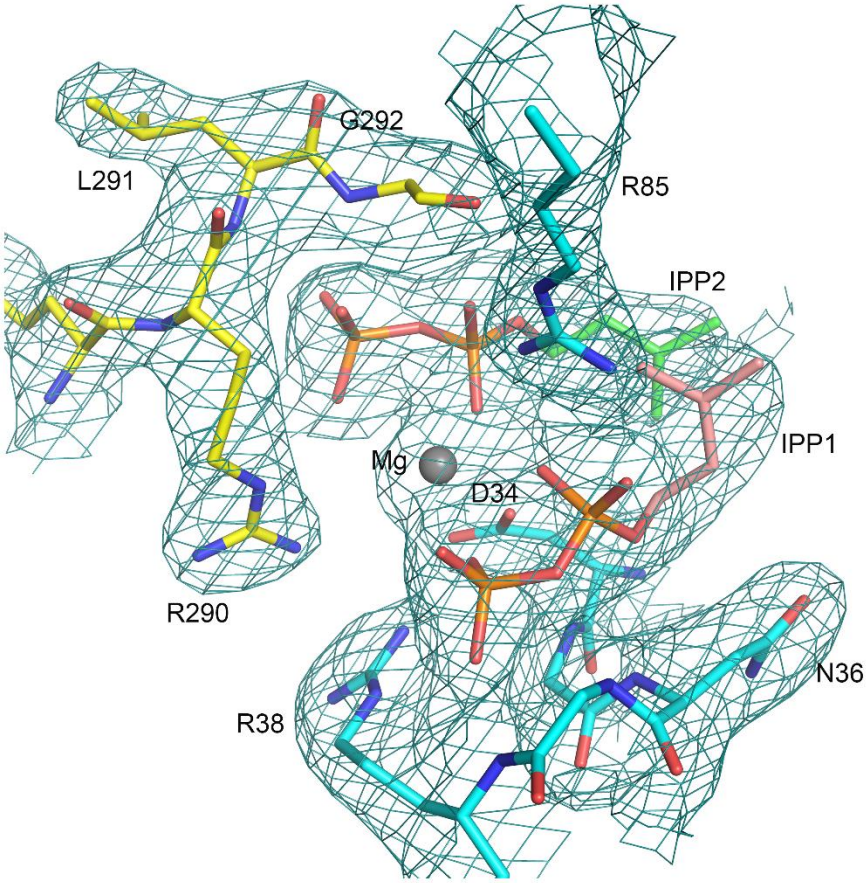

Figure S6. The final 2Fo-Fc map surrounding the bound ligands.

The electron density is contoured at 1.0 σ level. The oxygen atoms are colored red and phosphorus atoms are colored orange. The carbon atoms of IPP1 are colored salmon and those of IPP2 are in green. DHDDS residues involved in catalysis and substrate binding are shown in cyan, while those of NgBR are shown in yellow. Magnesium ion is depicted as a gray sphere.

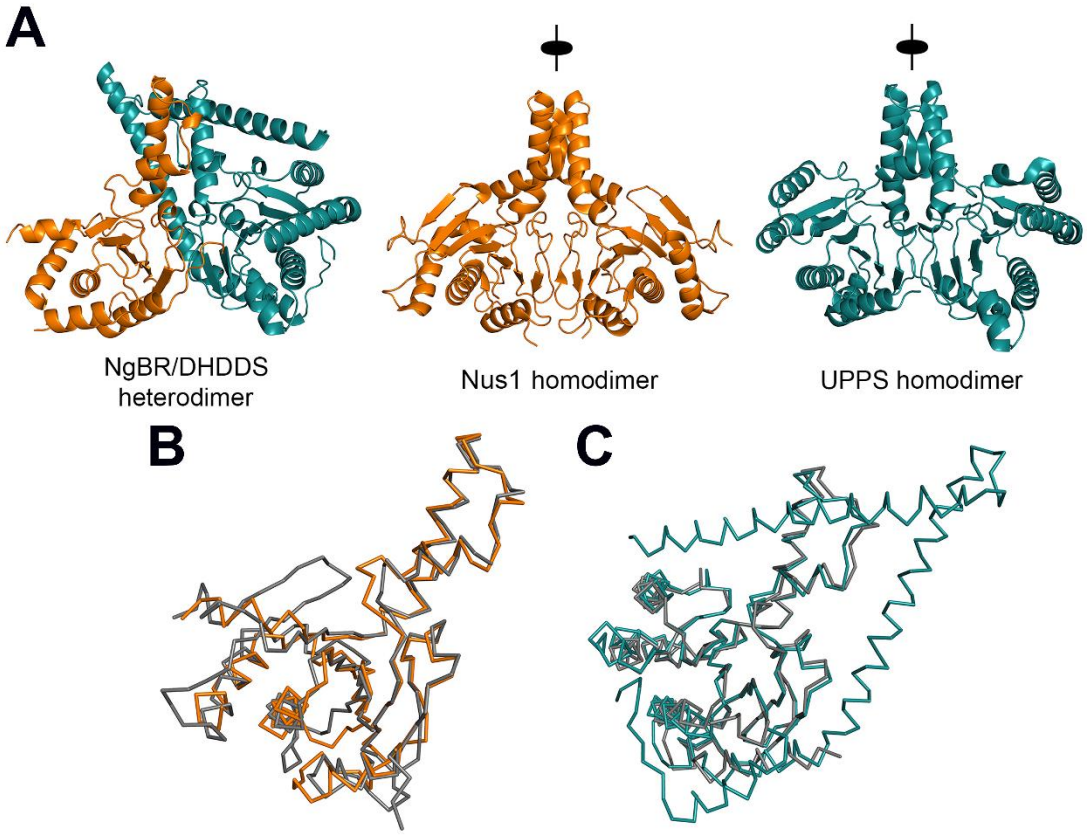

Figure S7. Comparison of different dimeric structures.

(A) Ribbon diagram of the heteromeric complex is shown. NgBR is colored in orange, and DHDDS is colored in deep teal. The heteromeric structure is compared with those of yeast NUS1 dimer (PDB 6JCN) colored in orange and *E. coli* UPPS (PDB 1X06) colored in deep teal.
(B) NgBR (orange) is superimposed on yeast NUS1 (gray) (C□ RMSD 1.8 Å). Wireframe diagram of C_α atoms is shown.
(C) DHDDS (deep teal) is superimposed on *E. coli* UPPS (gray) (C□ RMSD 1.2 Å).

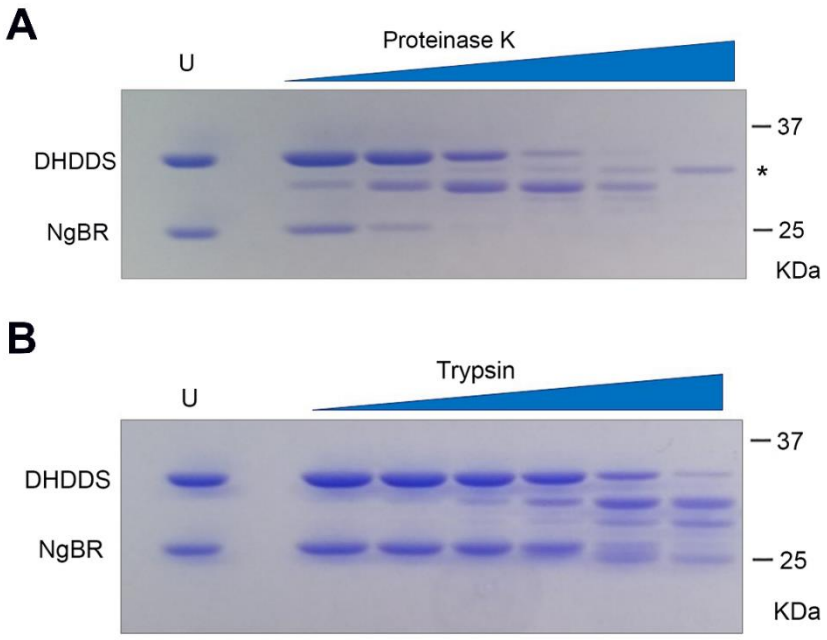

Figure S8. Limited proteolysis of NgBR/DHDDS complex.

Purified protein complex was incubated with increasing concentrations of proteinase k (A) or trypsin (B) (0.005, 0.01, 0.02, 0.04, 0.08, 0.16 mg/ml). Untreated protein sample is denoted as (U) and the location of proteinase k is indicated by the asterisks. The time course of degradation observed with both proteases is similar to that with thermolysin shown in fig.2B whereby NgBR cleavage occurs prior to DHDDS.

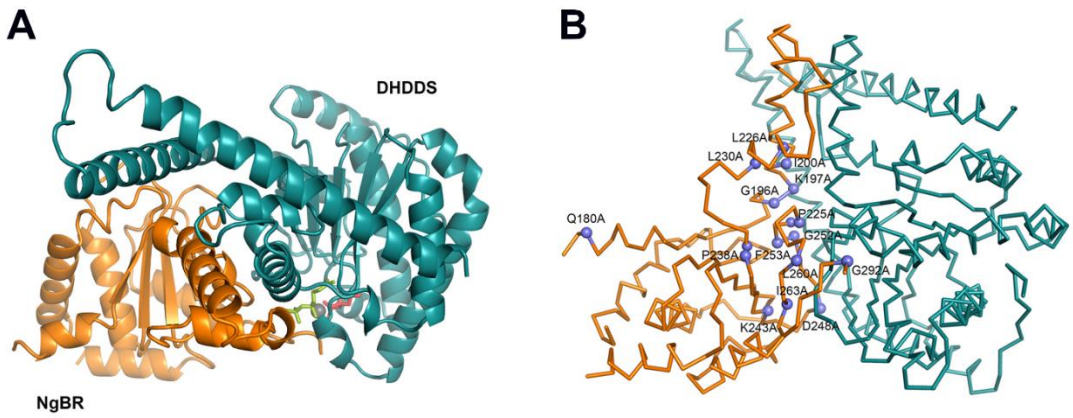

Figure S9. The dimeric interphase between NgBR and DHDDS.

(A) A top view of the heteromeric complex. The dimeric interface has a surface area of 2,029 $Å^2$. NgBR is colored in orange and DHDDS in deep teal.
(B) The position of the NgBR mutations described in Fig. 2B. I200A, L226A, L230A, G252A, F253A and P255A are most disruptive to dimerization, which is consistent with their location within the canonical dimer interface. The side chains of Lys-197 and Asp-248 participate in hydrogen-bonding across the dimer interface. Ile-263 and Gly-292 participate in hydrophobic contacts across the interface. However, K197A, D248A, I263A and G292A have a relatively small effect, suggesting that these interactions do not contribute significantly to dimer stability. Based on the bacterial UPPS structure, Gln-180 was predicted to also fall within the dimer interface. However, as revealed by the new heteromeric structure, this residue is distal to the interface, which explains why Q180A has no effect on dimerization. The remaining four mutations affect residues that are near the interface but do not directly contact DHDDS. G196A alters the packing of the interfacial □5 helix and thus influences dimer stability indirectly. The other three mutations (P238A, K243A, L260A) have no effect on dimerization.

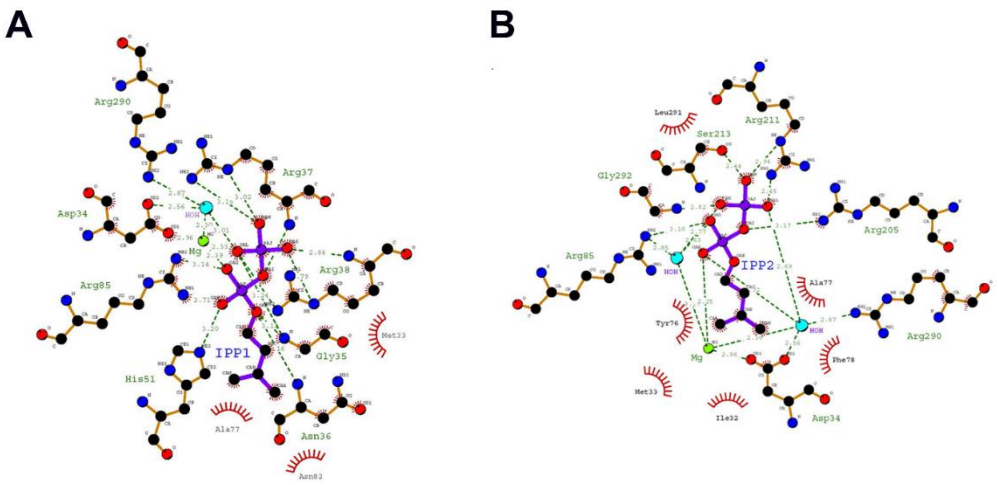

Figure S10. The complete binding interactions for IPP1 and IPP2.

2D representations of the binding interactions for IPP1 (A) and IPP2 (B) are shown (1). Nitrogen atoms are colored blue, oxygen atoms in red, carbon atoms in black and water molecules in turquoise. Phosphorus atoms and bonds of both ligands are shown in purple and non-ligand bonds are shown in orange. All hydrogen bonds are depicted by green dashed lines and labeled for distance.

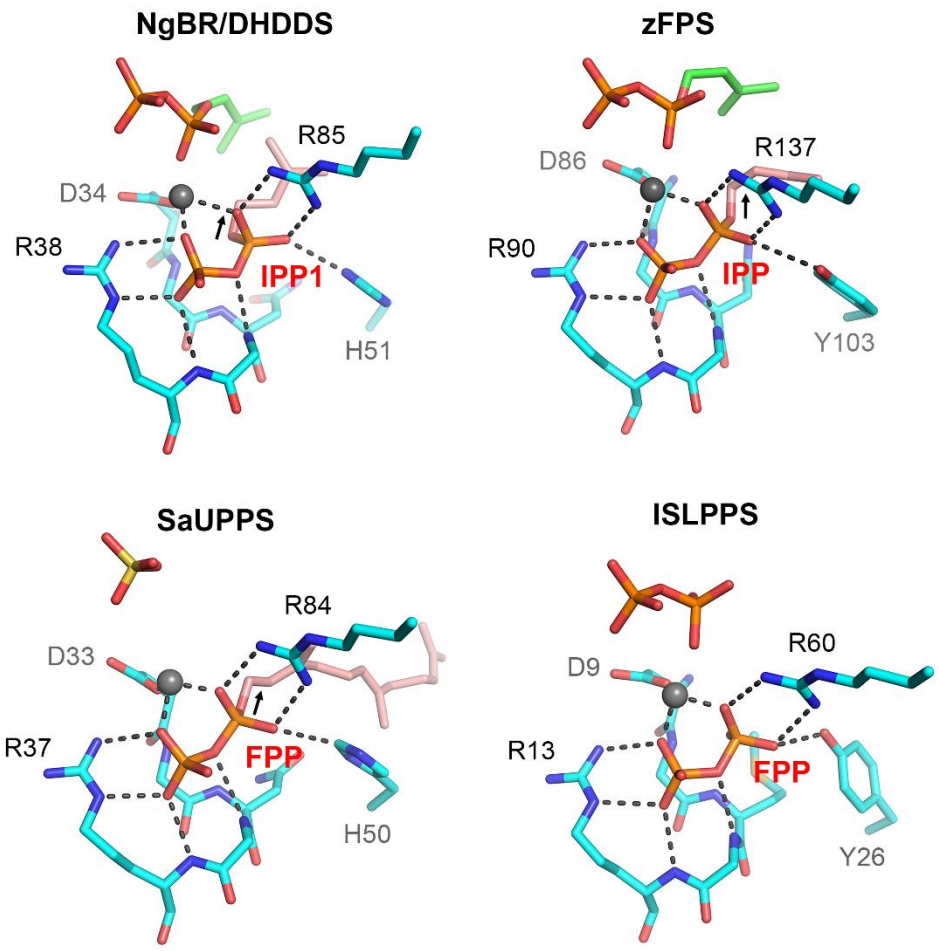

Figure S11. Structural comparison of the S1 site.

The S1 site involved in the binding of allylic substrate is compared among different *cis*-PTases including human NgBR/DHDDS complex, *cis*-PTase from tomato, denoted as zFPS (PDB ID 5HXP), *S. aureus* UPPS denoted as SaUPPS (PDB ID 4H8E) and isosesquilavandulyl diphosphate synthase denoted as ISLPPS (PDB ID 5XK6). Mg^{2+} ion is shown as gray sphere, conserved residues involved in binding of allylic pyrophosphate are colored in cyan and labeled, and hydrogen bonds are shown as black-dashed lines. Oxygen atoms are colored red, phosphorus atoms are in orange and nitrogen are in blue. The carbon atoms of the allylic substrate are shown in salmon and those for the homoallylic substrate are shown in green. His-51 in the human NgBR/DHDDS complex is sometimes replaced with tyrosine; in both cases, the side chain is involved in hydrogen bonding with α phosphate of the allylic substrate. His-50 in SaUPPS can also participate in hydrogen bonding if the imidazole ring is rotated 180 degrees.

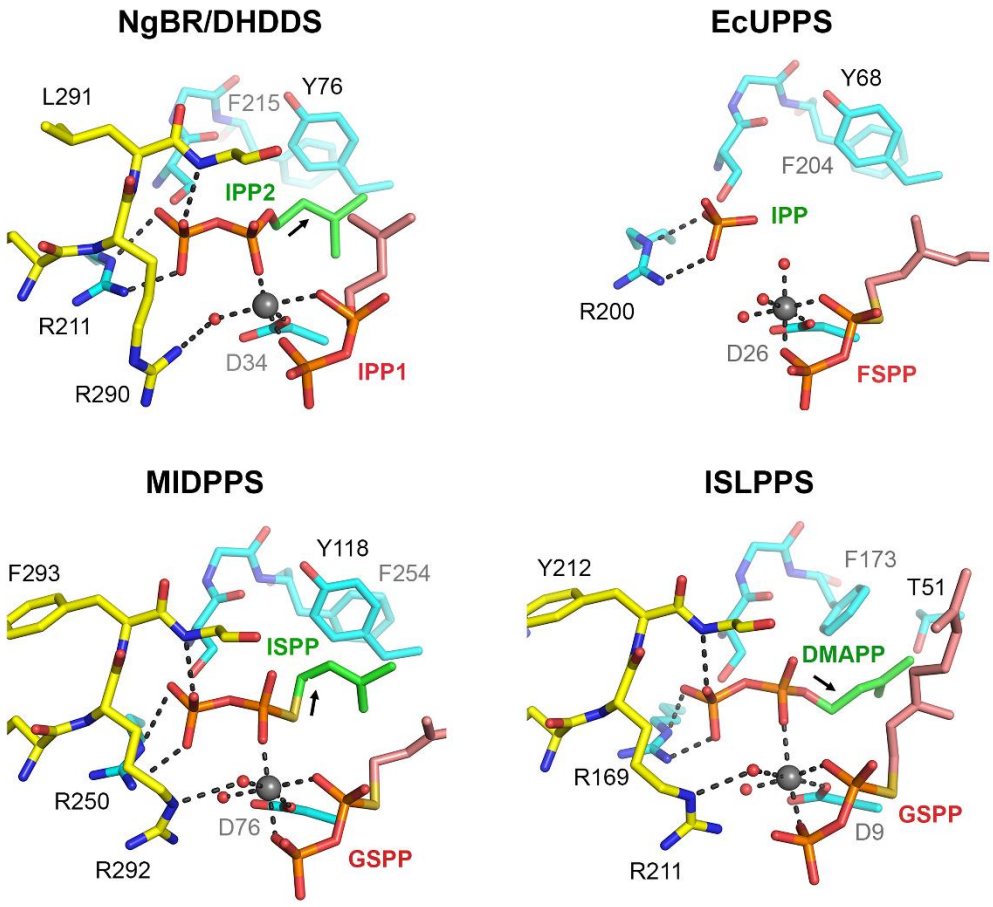

Figure S12. Structural comparison of the S2 site.

The S2 site involved in the binding of homoallylic substrate is compared among different *cis*-PTases including human NgBR/DHDDS complex, *cis*-PTase from *E.coli* UPPS, denoted as EcUPPS (PDB ID 1X06), *M. tuberculosis* UPPS Rv2361c denoted as MlDPPS (PDB ID 6IME) and isosesquilavandulyl diphosphate synthase denoted as ISLPPS (PDB ID 5XK9). Mg^{2+} ion is shown as gray sphere, conserved C-terminal -RXG- residues from NgBR and other corresponding monomers are colored in yellow while those for DHDDS are in cyan. Hydrogen bonds are shown as black-dashed lines. Oxygen atoms are colored red, phosphorus atoms are in orange and nitrogen atoms are in blue. The carbon atoms of the allylic substrate are shown in salmon and those for the homoallylic substrate are shown in green. The disordered -RXG- motif in EcUPPS results in an incomplete active site and misplaced IPP phosphate.

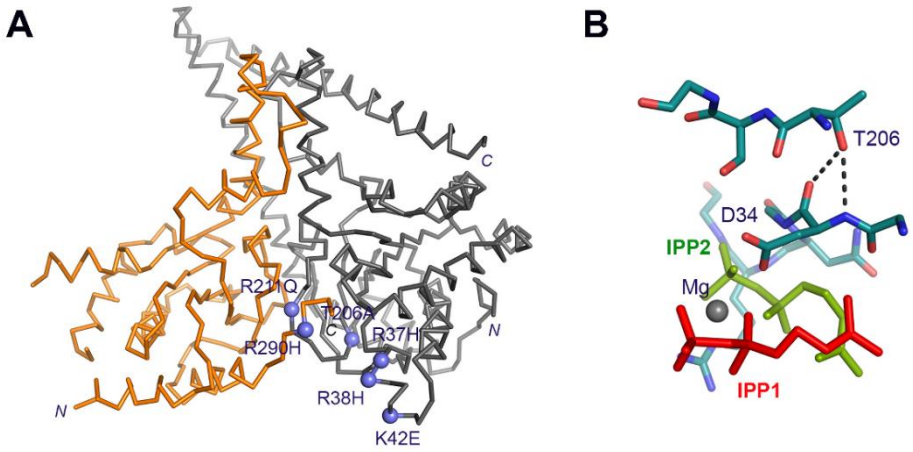

Figure S13. Missense mutations associated with CDG.

(A) CDG-causing NgBR and DHDDS mutations are indicated as purple spheres on the structure. NgBR is colored in orange and DHDDS in gray. The CDG mutations cluster around the active site of the complex. In DHDDS, those include: Arg-37, Arg-38, Lys-42, Thr-206, and Arg-211. In NgBR, Arg-290 is part of the conserved C-terminal -RXG- motif.
(B) The side chain of Thr-206 is involved in hydrogen bonding (shown as dashed lines) with the backbone amide and carbonyl of Asp-34. The carbon atoms are colored deep teal, nitrogen atoms colored blue and oxygen atoms colored red. IPP1 colored red, IPP2 colored green and the Mg^{2+} is shown as a gray sphere.

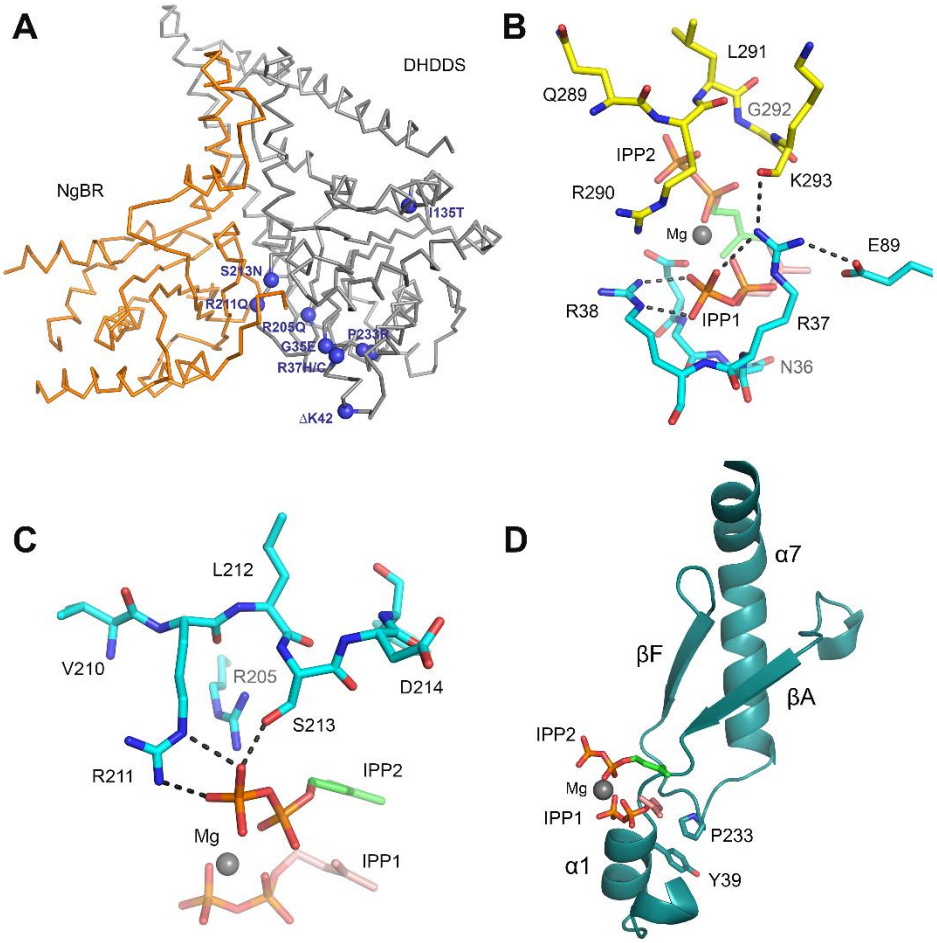

Figure S14. De novo DHDDS mutations associated with neurodegenerative disorder

(A) DHDDS mutations are indicated as purple spheres on the structure. NgBR is colored in orange and DHDDS in gray. Most of the mutations cluster around the active site of the complex, including S213N, R211Q, R205Q, G35E, P233R and R37H/C. An exception is I135T, which is distal to the active site.
(B) The side chain of R37 is involved in a network of interactions with the pyrophosphate moiety of the allylic substrate, the side chain of a conserved E89 on DHDDS, and the main chain amide of K293 from NgBR C-terminal region. The carbon atoms are colored deep teal, nitrogen atoms colored blue and oxygen atoms colored red. IPP1 colored red, IPP2 colored green and the Mg^{2+} is shown as a gray sphere.
(C) Side chains of R205, R211 and S213 are depicted at the S2 site, and are involved in salt bridging and hydrogen bonding with the pyrophosphate group of IPP substrate. Replacement of Arg residues with Gln will eliminate these salt bridges and thus weaken IPP binding. Substituting Ser with Asn might result in steric clashes with nearby residues, thereby destabilizing the structure.

(D) Ribbon diagram showing the side chain of P233 is involved in hydrophobic packing against Y39, which is located at α1 helix known to harbor residues important for FPP binding. A P233R mutation will disrupt such packing interaction and may destabilize α1 helix.

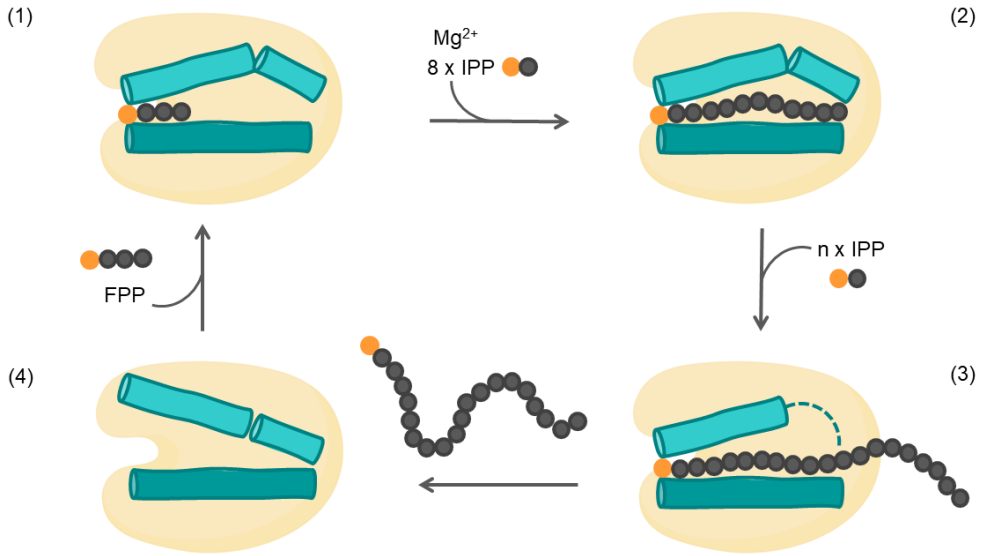

Figure S15. Plausible catalytic mechanism of the human NgBR/DHDDS complex

The synthesis of polyprenol pyrophosphate is initiated with the binding of FPP to the empty S1 site, followed by binding of Mg^{2+}-IPP complex to the S2 site. Two conformational changes might occur at this point: the first involves the α3 helix, which becomes more kinked to enhance hydrophobic interactions with the substrates. A second conformational change might involve a transient membrane binding facilitated by DHDDS α0 helix which will displace its N-terminal coil from the hydrophobic cavity between α2 and α3, rendering it accessible for chain elongation. After several rounds of condensations (~13 isoprene units incorporated), the product is extended outside the tunnel, thereby allowing the condensation of 6 more isoprene units. As the product becomes exposed, interaction with ER membrane will further destabilize the enzyme : product complex, hence facilitating product release. At this stage, another conformational change involving α3 helix might occur, and allow the release of the newly synthesized polyprenol pyrophosphate.

Table S1. Crystallographic statistics. The NgBR/DHDDS heterodimer was crystallized in space group R32.

Data Collection	
Wavelength, Å	0.979
Cell Dimensions, Å	a=b=185.7, c=113.4
[a]Resolution (Å)	40-2.3 (2.38-2.30)
Redundancy	14.7 (4.5)
Completeness (%)	95.0 (74.5)
$\langle I \rangle / \langle \sigma \rangle$	17.4 (0.9)
$CC_{1/2}$	0.997 (0.473)
[a,b]R_{pim}	0.036 (0.549)
Refinement	
Unique reflections	29,756
Number of Atoms	4,036
Protein	3,901
Ligand	29
Solvent	106
[c]R_{work}/R_{free}	0.212/0.255
Mean B-value (Å^2)	78.8
Protein	79.0
Ligand	66.5
Solvent	75.2
r.m.s. deviations	
Bond lengths (Å)	0.004
Bond angles (°)	1.133
[d]Ramachandran (f, a, o)	96%, 4%, 0%
PDB accession code	6W2L

REFERENCES

1. Crowell DN & Huizinga DH (2009) Protein isoprenylation: the fat of the matter. *Trends Plant Sci* 14(3):163-170.

2. Grabińska KA, Park EJ, & Sessa WC (2016) cis-Prenyltransferase: New Insights into Protein Glycosylation, Rubber Synthesis, and Human Diseases. *J Biol Chem* 291(35):18582-18590.

3. Lange BM, Rujan T, Martin W, & Croteau R (2000) Isoprenoid biosynthesis: The evolution of two ancient and distinct pathways across genomes. *Proceedings of the National Academy of Sciences* 97(24):13172-13177.

4. Nowicka B & Kruk J (2010) Occurrence, biosynthesis and function of isoprenoid quinones. *Biochim Biophys Acta* 1797(9):1587-1605.

5. Santner A, Calderon-Villalobos LIA, & Estelle M (2009) Plant hormones are versatile chemical regulators of plant growth. *Nature Chemical Biology* 5(5):301-307.

6. Takahashi S & Koyama T (2006) Structure and function of cis-prenyl chain elongating enzymes. *Chem Rec* 6(4):194-205.

7. Miziorko HM (2011) Enzymes of the mevalonate pathway of isoprenoid biosynthesis. *Arch Biochem Biophys* 505(2):131-143.

8. Rohmer M, Grosdemange-Billiard C, Seemann M, & Tritsch D (2004) Isoprenoid biosynthesis as a novel target for antibacterial and antiparasitic drugs. *Curr Opin Investig Drugs* 5(2):154-162.

9. Grabińska KA, Edani BH, Park EJ, Kraehling JR, & Sessa WC (2017) A conserved C-terminal RXG motif in the NgBR subunit of cis-prenyltransferase is critical for prenyltransferase activity. *J Biol Chem* 292(42):17351-17361.

10. Chen C-C, *et al.* (2020) Versatile cis-isoprenyl Diphosphate Synthase Superfamily Members in Catalyzing Carbon–Carbon Bond Formation. *ACS Catalysis* 10(8):4717-4725.

11. Koyama T (1999) Molecular analysis of prenyl chain elongating enzymes. *Biosci Biotechnol Biochem* 63(10):1671-1676.

12. Shimizu N, Koyama T, & Ogura K (1998) Molecular cloning, expression, and purification of undecaprenyl diphosphate synthase. No sequence similarity between E- and Z-prenyl diphosphate synthases. *J Biol Chem* 273(31):19476-19481.

13. Teng KH & Liang PH (2012) Structures, mechanisms and inhibitors of undecaprenyl diphosphate synthase: a cis-prenyltransferase for bacterial peptidoglycan biosynthesis. *Bioorg Chem* 43:51-57.

14. Apfel CM, Takács B, Fountoulakis M, Stieger M, & Keck W (1999) Use of genomics to identify bacterial undecaprenyl pyrophosphate synthetase: cloning, expression, and characterization of the essential uppS gene. *J Bacteriol* 181(2):483-492.

15. Sato M, *et al.* (1999) The yeast RER2 gene, identified by endoplasmic reticulum protein localization mutations, encodes cis-prenyltransferase, a key enzyme in dolichol synthesis. *Mol Cell Biol* 19(1):471-483.

16. Ogawa T, Emi K-i, Koga K, Yoshimura T, & Hemmi H (2016) A cis-prenyltransferase from Methanosarcina acetivorans catalyzes both head-to-tail and nonhead-to-tail prenyl condensation. *The FEBS Journal* 283(12):2369-2383.

17. Liu M, *et al.* (2016) Structure and Function of a "Head-to-Middle" Prenyltransferase: Lavandulyl Diphosphate Synthase. *Angew Chem Int Ed Engl* 55(15):4721-4724.

18. Ozaki T, Zhao P, Shinada T, Nishiyama M, & Kuzuyama T (2014) Cyclolavandulyl Skeleton Biosynthesis via Both Condensation and Cyclization Catalyzed by an Unprecedented Member of the cis-Isoprenyl Diphosphate Synthase Superfamily. *Journal of the American Chemical Society* 136(13):4837-4840.

19. Cunillera N, Arró M, Forés O, Manzano D, & Ferrer A (2000) Characterization of dehydrodolichyl diphosphate synthase of Arabidopsis thaliana, a key enzyme in dolichol biosynthesis. *FEBS Lett* 477(3):170-174.

20. Endo S, Zhang Y-W, Takahashi S, & Koyama T (2003) Identification of human dehydrodolichyl diphosphate synthase gene. *Biochimica et Biophysica Acta (BBA) - Gene Structure and Expression* 1625(3):291-295.

21. Oh SK, Han KH, Ryu SB, & Kang H (2000) Molecular cloning, expression, and functional analysis of a cis-prenyltransferase from Arabidopsis thaliana. Implications in rubber biosynthesis. *J Biol Chem* 275(24):18482-18488.

22. Shridas P, Rush JS, & Waechter CJ (2003) Identification and characterization of a cDNA encoding a long-chain cis-isoprenyltranferase involved in dolichyl monophosphate biosynthesis in the ER of brain cells. *Biochem Biophys Res Commun* 312(4):1349-1356.

23. Buczkowska A, Swiezewska E, & Lefeber DJ (2015) Genetic defects in dolichol metabolism. *J Inherit Metab Dis* 38(1):157-169.

24. Concha N, *et al.* (2016) Discovery and Characterization of a Class of Pyrazole Inhibitors of Bacterial Undecaprenyl Pyrophosphate Synthase. *Journal of Medicinal Chemistry* 59(15):7299-7304.

25. Jukič M, Rožman K, Sova M, Barreteau H, & Gobec S (2019) Anthranilic Acid Inhibitors of Undecaprenyl Pyrophosphate Synthase (UppS), an Essential Enzyme for Bacterial Cell Wall Biosynthesis. *Frontiers in Microbiology* 9:3322.

26. Farha MA, *et al.* (2015) Antagonism screen for inhibitors of bacterial cell wall biogenesis uncovers an inhibitor of undecaprenyl diphosphate synthase. *Proc Natl Acad Sci U S A* 112(35):11048-11053.

27. Guo R-T, *et al.* (2007) Bisphosphonates target multiple sites in both cis- and trans-prenyltransferases. *Proceedings of the National Academy of Sciences* 104(24):10022-10027.

28. Zhu W, *et al.* (2013) Antibacterial drug leads targeting isoprenoid biosynthesis. *Proceedings of the National Academy of Sciences* 110(1):123-128.

29. Akhtar TA, *et al.* (2013) The tomato cis-prenyltransferase gene family. *Plant J* 73(4):640-652.

30. Grabińska KA, *et al.* (2010) Molecular characterization of the cis-prenyltransferase of Giardia lamblia. *Glycobiology* 20(7):824-832.

31. Hemmi H, Yamashita S, Shimoyama T, Nakayama T, & Nishino T (2001) Cloning, Expression, and Characterization ofcis-Polyprenyl Diphosphate Synthase from the Thermoacidophilic Archaeon Sulfolobus acidocaldarius. *Journal of Bacteriology* 183(1):401-404.

32. Kaur D, Brennan PJ, & Crick DC (2004) Decaprenyl diphosphate synthesis in Mycobacterium tuberculosis. *J Bacteriol* 186(22):7564-7570.

33. Löw P, *et al.* (1991) The mevalonate pathway in the bloodstream form of Trypanosoma brucei. Identification of dolichols containing 11 and 12 isoprene residues. *J Biol Chem* 266(29):19250-19257.

34. Schilmiller AL, *et al.* (2009) Monoterpenes in the glandular trichomes of tomato are synthesized from a neryl diphosphate precursor rather than geranyl diphosphate. *Proceedings of the National Academy of Sciences* 106(26):10865-10870.

35. Schulbach MC, Brennan PJ, & Crick DC (2000) Identification of a short (C15) chain Z-isoprenyl diphosphate synthase and a homologous long (C50) chain isoprenyl diphosphate synthase in Mycobacterium tuberculosis. *J Biol Chem* 275(30):22876-22881.

36. Taguchi Y, Fujinami D, & Kohda D (2016) Comparative Analysis of Archaeal Lipid-linked Oligosaccharides That Serve as Oligosaccharide Donors for Asn Glycosylation. *J Biol Chem* 291(21):11042-11054.

37. Brasher MI, *et al.* (2015) A two-component enzyme complex is required for dolichol biosynthesis in tomato. *Plant J* 82(6):903-914.

38. Emi K-i, Sompiyachoke K, Okada M, & Hemmi H (2019) A heteromeric cis-prenyltransferase is responsible for the biosynthesis of glycosyl carrier lipids in Methanosarcina mazei. *Biochemical and Biophysical Research Communications* 520(2):291-296.

39. Park EJ, *et al.* (2014) Mutation of Nogo-B receptor, a subunit of cis-prenyltransferase, causes a congenital disorder of glycosylation. *Cell Metab* 20(3):448-457.

40. Epping J, *et al.* (2015) A rubber transferase activator is necessary for natural rubber biosynthesis in dandelion. *Nature Plants* 1(5):15048.

41. Qu Y, *et al.* (2015) A lettuce (Lactuca sativa) homolog of human Nogo-B receptor interacts with cis-prenyltransferase and is necessary for natural rubber biosynthesis. *J Biol Chem* 290(4):1898-1914.

42. Sato M, Fujisaki S, Sato K, Nishimura Y, & Nakano A (2001) Yeast Saccharomyces cerevisiae has two cis-prenyltransferases with different properties and localizations. Implication for their distinct physiological roles in dolichol synthesis. *Genes Cells* 6(6):495-506.

43. Schenk B, Rush JS, Waechter CJ, & Aebi M (2001) An alternative cis-isoprenyltransferase activity in yeast that produces polyisoprenols with chain lengths similar to mammalian dolichols. *Glycobiology* 11(1):89-98.

44. Miao RQ, *et al.* (2006) Identification of a receptor necessary for Nogo-B stimulated chemotaxis and morphogenesis of endothelial cells. *Proceedings of the National Academy of Sciences* 103(29):10997-11002.

45. Harrison KD, *et al.* (2009) Nogo-B receptor stabilizes Niemann-Pick type C2 protein and regulates intracellular cholesterol trafficking. *Cell Metab* 10(3):208-218.

46. Harrison KD, *et al.* (2011) Nogo-B receptor is necessary for cellular dolichol biosynthesis and protein N-glycosylation. *EMBO J* 30(12):2490-2500.

47. Kwon M, Kwon EJG, & Ro DK (2016) Chapter Six - cis-Prenyltransferase and Polymer Analysis from a Natural Rubber Perspective. *Methods in Enzymology*, ed O'Connor SE (Academic Press), Vol 576, pp 121-145.

48. Fujihashi M, *et al.* (2001) Crystal structure of cis-prenyl chain elongating enzyme, undecaprenyl diphosphate synthase. *Proceedings of the National Academy of Sciences* 98(8):4337-4342.

49. Chan Y-T, *et al.* (2017) Crystal Structure and Potential Head-to-Middle Condensation Function of a Z,Z-Farnesyl Diphosphate Synthase. *ACS Omega* 2(3):930-936.

50. Guo RT, *et al.* (2005) Crystal structures of undecaprenyl pyrophosphate synthase in complex with magnesium, isopentenyl pyrophosphate, and farnesyl thiopyrophosphate: roles of the metal ion and conserved residues in catalysis. *J Biol Chem* 280(21):20762-20774.

51. Wang W, *et al.* (2008) The structural basis of chain length control in Rv1086. *J Mol Biol* 381(1):129-140.

52. Chang SY, Ko TP, Liang PH, & Wang AH (2003) Catalytic mechanism revealed by the crystal structure of undecaprenyl pyrophosphate synthase in complex with sulfate, magnesium, and triton. *J Biol Chem* 278(31):29298-29307.

53. Kharel Y, Zhang Y-W, Fujihashi M, Miki K, & Koyama T (2001) Identification of Significant Residues for Homoallylic Substrate Binding of Micrococcus luteus B-P 26 Undecaprenyl Diphosphate Synthase. *Journal of Biological Chemistry* 276(30):28459-28464.

54. Pan J-J, Yang L-W, & Liang P-H (2000) Effect of Site-Directed Mutagenesis of the Conserved Aspartate and Glutamate on E. coli Undecaprenyl Pyrophosphate Synthase Catalysis. *Biochemistry* 39(45):13856-13861.

55. Lisnyansky Bar-El M, *et al.* (2019) Structural Characterization of Full-Length Human Dehydrodolichyl Diphosphate Synthase Using an Integrative Computational and Experimental Approach. *Biomolecules* 9(11).

56. Yamashita S, *et al.* (2016) Identification and reconstitution of the rubber biosynthetic machinery on rubber particles from Hevea brasiliensis. *Elife* 5.

57. Lakusta AM, *et al.* (2019) Molecular Studies of the Protein Complexes Involving Cis-Prenyltransferase in Guayule (Parthenium argentatum), an Alternative Rubber-Producing Plant. *Frontiers in Plant Science* 10(165).

58. Emi KI, Sompiyachoke K, Okada M, & Hemmi H (2019) A heteromeric cis-prenyltransferase is responsible for the biosynthesis of glycosyl carrier lipids in Methanosarcina mazei. *Biochem Biophys Res Commun* 520(2):291-296.

59. Den K, *et al.* (2019) Recurrent NUS1 canonical splice donor site mutation in two unrelated individuals with epilepsy, myoclonus, ataxia and scoliosis - a case report. *BMC Neurology* 19(1):253.

60. Hamdan FF, *et al.* (2017) High Rate of Recurrent De Novo Mutations in Developmental and Epileptic Encephalopathies. *Am J Hum Genet* 101(5):664-685.

61. Sabry S, *et al.* (2016) A case of fatal Type I congenital disorders of glycosylation (CDG I) associated with low dehydrodolichol diphosphate synthase (DHDDS) activity. *Orphanet J Rare Dis* 11(1):84.

62. Zelinger L, *et al.* (2011) A missense mutation in DHDDS, encoding dehydrodolichyl diphosphate synthase, is associated with autosomal-recessive retinitis pigmentosa in Ashkenazi Jews. *Am J Hum Genet* 88(2):207-215.

63. Züchner S, *et al.* (2011) Whole-exome sequencing links a variant in DHDDS to retinitis pigmentosa. *Am J Hum Genet* 88(2):201-206.

64. Gao J, *et al.* (2018) "Head-to-Middle" and "Head-to-Tail" cis-Prenyl Transferases: Structure of Isosesquilavandulyl Diphosphate Synthase. *Angew Chem Int Ed Engl* 57(3):683-687.

65. Ko TP, *et al.* (2019) Substrate-analogue complex structure of Mycobacterium tuberculosis decaprenyl diphosphate synthase. *Acta Crystallogr F Struct Biol Commun* 75(Pt 4):212-216.

66. Wen R, Lam BL, & Guan Z (2013) Aberrant dolichol chain lengths as biomarkers for retinitis pigmentosa caused by impaired dolichol biosynthesis. *J Lipid Res* 54(12):3516-3522.

67. Steward CA, *et al.* (2019) Re-annotation of 191 developmental and epileptic encephalopathy-associated genes unmasks de novo variants in SCN1A. *npj Genomic Medicine* 4(1):31.

68. Milani D, *et al.* (2016) Insights into 6q21-q22: Refinement of the critical region for acro-cardio-facial syndrome. *Congenital Anomalies* 56(4):187-189.

69. Szafranski P, *et al.* (2015) 6q22.1 microdeletion and susceptibility to pediatric epilepsy. *Eur J Hum Genet* 23(2):173-179.

70. Guo JF, *et al.* (2018) Coding mutations in NUS1 contribute to Parkinson's disease. *Proc Natl Acad Sci U S A* 115(45):11567-11572.

71. PULA B, *et al.* (2014) Nogo-B Receptor Expression Correlates Negatively with Malignancy Grade and Ki-67 Antigen Expression in Invasive Ductal Breast Carcinoma. *Anticancer Research* 34(9):4819-4828.

72. Wang B, *et al.* (2013) Expression of NgBR is highly associated with estrogen receptor alpha and survivin in breast cancer. *PLoS One* 8(11):e78083.

73. Zhang R, Tang BS, & Guo JF (2020) Research advances on neurite outgrowth inhibitor B receptor. *J Cell Mol Med* 24(14):7697-7705.

74. Zhao B, *et al.* (2015) Comprehensive proteome quantification reveals NgBR as a new regulator for epithelial-mesenchymal transition of breast tumor cells. *J Proteomics* 112:38-52.

75. Banerjee DK (2012) N-glycans in cell survival and death: cross-talk between glycosyltransferases. *Biochim Biophys Acta* 1820(9):1338-1346.

76. Janik ME, Lityńska A, & Vereecken P (2010) Cell migration-the role of integrin glycosylation. *Biochim Biophys Acta* 1800(6):545-555.

77. Zhao B, *et al.* (2017) The Nogo-B receptor promotes Ras plasma membrane localization and activation. *Oncogene* 36(24):3406-3416.

78. Gao P, *et al.* (2018) Nogo-B receptor increases the resistance to tamoxifen in estrogen receptor-positive breast cancer cells. *Breast Cancer Research* 20(1):112.

79. Jin Y, *et al.* (2018) Nogo-B receptor increases the resistance of estrogen receptor positive breast cancer to paclitaxel. *Cancer Lett* 419:233-244.

80. PULA B, *et al.* (2014) Expression of Nogo Isoforms and Nogo-B Receptor (NgBR) in Non-small Cell Lung Carcinomas. *Anticancer Research* 34(8):4059-4068.

81. Wu D, *et al.* (2018) Nogo-B receptor promotes epithelial-mesenchymal transition in non-small cell lung cancer cells through the Ras/ERK/Snail1 pathway. *Cancer Lett* 418:135-146.

82. Park EJ, Grabińska KA, Guan Z, & Sessa WC (2016) NgBR is essential for endothelial cell glycosylation and vascular development. *EMBO Rep* 17(2):167-177.

83. Zhao B, *et al.* (2010) Nogo-B receptor is essential for angiogenesis in zebrafish via Akt pathway. *Blood* 116(24):5423-5433.

84. Ma J, *et al.* (2019) Structural insights to heterodimeric cis-prenyltransferases through yeast dehydrodolichyl diphosphate synthase subunit Nus1. *Biochem Biophys Res Commun* 515(4):621-626.

85. Otwinowski Z & Minor W (1997) [20] Processing of X-ray diffraction data collected in oscillation mode. *Methods in Enzymology*, (Academic Press), Vol 276, pp 307-326.

86. Winn MD, *et al.* (2011) Overview of the CCP4 suite and current developments. *Acta Crystallogr D Biol Crystallogr* 67(Pt 4):235-242.

87. Emsley P, Lohkamp B, Scott WG, & Cowtan K (2010) Features and development of Coot. *Acta Crystallographica Section D* 66(4):486-501.

88. Holcomb J, *et al.* (2018) SAXS analysis of a soluble cytosolic NgBR construct including extracellular and transmembrane domains. *PLoS One* 13(1):e0191371.

89. Malwal SR, *et al.* (2018) Catalytic Role of Conserved Asparagine, Glutamine, Serine, and Tyrosine Residues in Isoprenoid Biosynthesis Enzymes. *ACS Catalysis* 8(5):4299-4312.

90. Kimchi A, *et al.* (2018) Nonsyndromic Retinitis Pigmentosa in the Ashkenazi Jewish Population: Genetic and Clinical Aspects. *Ophthalmology* 125(5):725-734.

91. Fedorow H, *et al.* (2005) Dolichol is the major lipid component of human substantia nigra neuromelanin. *J Neurochem* 92(4):990-995.

92. Ward WC, *et al.* (2007) Identification and quantification of dolichol and dolichoic acid in neuromelanin from substantia nigra of the human brain. *J Lipid Res* 48(7):1457-1462.

93. Cherian S, Ryu SB, & Cornish K (2019) Natural rubber biosynthesis in plants, the rubber transferase complex, and metabolic engineering progress and prospects. *Plant Biotechnol J* 17(11):2041-2061.

94. Hoffmann R, Grabińska K, Guan Z, Sessa WC, & Neiman AM (2017) Long-Chain Polyprenols Promote Spore Wall Formation in Saccharomyces cerevisiae. *Genetics* 207(4):1371-1386.

95. Voss NR & Gerstein M (2010) 3V: cavity, channel and cleft volume calculator and extractor. *Nucleic Acids Res* 38(Web Server issue):W555-562.

96. CHEN Annie P-C, *et al.* (2005) Substrate and product specificities of cis-type undecaprenyl pyrophosphate synthase. *Biochemical Journal* 386(1):169-176.

97. Chen YH, Chen AP, Chen CT, Wang AH, & Liang PH (2002) Probing the conformational change of Escherichia coli undecaprenyl pyrophosphate synthase during catalysis using an inhibitor and tryptophan mutants. *J Biol Chem* 277(9):7369-7376.

98. Ko TP, *et al.* (2001) Mechanism of product chain length determination and the role of a flexible loop in Escherichia coli undecaprenyl-pyrophosphate synthase catalysis. *J Biol Chem* 276(50):47474-47482.

99. Bar-El ML, *et al.* (2020) Structural basis of heterotetrameric assembly and disease mutations in the human cis-prenyltransferase complex. *Nat Commun* 11(1):5273-5273.

100. Fliesler SJ, Kotla P, Ramachandra Rao S, & Pittler SJ (2019) Lack of overt pathology in a K42E knock-in mouse model of retinitis pigmentosa (RP59). *Investigative Ophthalmology & Visual Science* 60(9):450-450.

101. DeRamus ML, *et al.* (2020) Selective Ablation of Dehydrodolichyl Diphosphate Synthase in Murine Retinal Pigment Epithelium (RPE) Causes RPE Atrophy and Retinal Degeneration. *Cells* 9(3):771.

102. Ramachandra Rao S, *et al.* (2020) Retinal Degeneration Caused by Rod-Specific Dhdds Ablation Occurs without Concomitant Inhibition of Protein N-Glycosylation. *iScience* 23(6):101198.

103. Wen R, *et al.* (2014) Knock-down DHDDS expression induces photoreceptor degeneration in zebrafish. *Adv Exp Med Biol* 801:543-550.